UNIVERSITY OF CALIFORNIA

Los Angeles

# Elastic Stretchability of Conjugated Polymer Blends

A dissertation submitted in partial satisfaction of the

requirements for the degree Doctor of Philosophy

in Materials Science and Engineering

by

Huier Gao

2017

ABSTRACT OF THE DISSERTATION

Elastic stretchability of conjugated polymer blends

by

Huier Gao

Doctor of Philosophy in Materials Science and Engineering

University of California, Los Angeles, 2017

Professor Qibing Pei, Chair

Fabricating fully stretchable thin film electronic devices entails innovation fundamentally new materials and modification of device architecture. My research has focused on employing polymer light emitting electrochemical cells (PLECs) as the device architecture, and exploring morphological control in conjugated polymer blends as a novel approach to obtain semiconducting materials with elastic stretchability.

PLECs are based on a conjugated polymer and solid electrolyte blend sandwiched between a pair of electrodes to form in-situ light emitting p-i-n junction. The junction formation is an expedient way to reduce interfacial energy, leading to the insensitivity of the device operation with regard to the thickness of the active layer and work function of electrode materials. These features help simplify the device architecture and the fabrication process, and therefore, the PLECs are an attractive platform to investigate the stretchability of electronic materials and demonstrate stretchable light emitting devices.

An efficient PLEC has been demonstrated with a thin-film electroluminescent polymer

sandwiched between two opposite electrodes. The electroluminescent layer is a blend of a soluble alkyloxy phenyl substituted poly(1,4-phenylene vinylene) (SY-PPV) with an ionically conductive medium exoxylated trimethylolpropanetriacrylate (ETPTA), and lithium trifluoromethanesulfonate (LiTf). The concentration of lithium salt plays an important role in the device performance, in terms of lifetime, and turn-on speed. A maximum current efficiency of 5.9 cd/A and luminance stabilized at 1500 cd/$m^2$ were acquired at 4 wt% salt and 15 wt% ionic conductor concentration. The addition of poly (ethylene oxide) (PEO) as ionic conductive source reduced the stability of PLEC operation due to the severe phase separation issue, but would be a benefit to enhance stretchability.

Conjugated polymers containing long-chain alkyl side groups for solubility are generally unstretchable: large strain induces crack formation, fracture, or plastic deformation. A soluble bright yellow light emission conjugated polymer, SY-PPV, admixed with ionically conductive mediums containing PEO and ETPTA, and LiTf can form an interpenetrating polymer network (IPN) to impart elastomeric deformability to a conjugated polymer. The spin-cast blend film formed an IPN morphology wherein SY-PPV forms a porous network with pores filled by the ionic medium. No global polarization of the SY-PPV chains was observed at strains up to 100% as the dichroic ratios of absorption and photoluminescence spectra remain close to 1. Light emitting devices based on the blend sandwiched between two stretchable transparent composite electrodes could be stretched by up to 140% strain. No electroluminescence polarization was observed.

Stimulated by the compliance of the stretchable PLEC devices, thin-film polymer solar cell comprising an elastically stretchable polymer blend was also demonstrated. The photovoltaic blend consists of [6,6]-phenyl-C71-butyric acid methyl ester ($PC_{71}BM$) and poly(thieno[3,4-b]-thiophene/benzodithiophene) (PTB7) and is sandwiched between a pair of stretchable transparent electrodes. The use of a high boiling point additive, 1,8-diiodooctane

(DIO) in the formation of the blend film not only improves the photovoltaic efficiency, but also renders the blend stretchable. The power conversion efficiency of the resulting solar cell device was 3.48%, and increased to 3.67% after one cycle of stretching to 50% strain. The cells could be stretched by as much as 100% strain. Microstructural analysis showed that the spin-cast blend film formed a uniform bulk heterojunction morphology where the $PC_{71}BM$ domain is present as small grains. The free volume left behind from DIO evaporation is crucial to the stretchability of the OPV blend. No global polarization of the PTB7 chains was observed when strain is released as the dichroic ratio remains close to 1.

Overall, this study shows that morphological control of polymer blends is an effective approach to render otherwise non-stretchable conjugated polymers into highly stretchable material while largely retaining the polymers electronic properties.

The dissertation of Huier Gao is approved.

Lihua Jin

Yang Yang

Yu Huang

Qibing Pei, Committee Chair

University of California, Los Angeles

2017

Dedicated to my beloved and always supportive parents,

Xiaoling Cheng and Yaohui Gao.

# TABLE OF CONTENTS

# LIST OF FIGURES

# LIST OF TABLES

# ACKNOWLEGEMENTS

I would like to take this opportunity to thank all the people who ever helped me in various ways during the past few years. I would like to pass my gratitude to my advisor, Dr. Qibing Pei, for his knowledge, and guidance through my time at the University of California, Los Angeles. I will forever appreciate the research experience and knowledge I have gained while working in his lab. I thank my doctoral committee members: Dr. Yang Yang, Dr. Yu Huang, and Dr. Lihua Jin. I would also acknowledge Dr. Adam Stieg for training and valuable discussion in PeakForce QNM experiments.

Chapter 3 is a version of "H. Gao, S. Chen, J. Liang, Q. Pei, Elastomeric light emitting polymer enhanced by interpenetrating networks, ACS Appl. Mater. Interfaces. 2016, 8, 32504-32511", reuse permission granted by American Chemical Society.

Chapter 4.3.1 is part of the work on stretchable organic solar cells done by Dr. Lu Li.

I would also like to acknowledge my friends and labmates. Thank all the previous and current group members, Dr. Zhibin Yu, Dr. Jiajie Liang, Dr. Si Chen, Dr. Wei Hu, Dr. Yan Xiong, Dr. Fangchao Zhao, Ms. Shu-Yu Chou, Mr. Chao Liu, and Mr. Tibor Hajagos, for sharing with me their experience and knowledge. From the insightful conversations about research to the fun times we had, you have made my experience enjoyable. I truly believe I have made not only connections for the future, but friends as well. I will miss every one of you.

Lastly, I would like to thank my parents. Thank you for your unwavering love and support as I reached for my goals. Without your firmly support, I would not be where I am today. You have always encouraged me to do my best and achieve whatever I set my mind to. I hope to continue to make you proud.

# VITA

| | |
|---|---|
| 2009 | B.S.<br>Department of Materials Science and Engineering<br>Donghua University<br>Shanghai, China |
| 2011 | M.S.<br>Materials Science and Engineering<br>University of California, Los Angeles<br>Los Angeles, CA |
| 2013-2017 | Ph.D. Candidate<br>Materials Science and Engineering<br>University of California, Los Angeles<br>Los Angeles, CA |

# Chapter 1 Introduction

## 1.1 Electroluminescent materials

Electroluminescent (EL) materials generate light through solid-state luminescent materials as a result of electrical excitation. A vast majority of organic EL is attributed to the charge injection through the electrode interface and recombination of the injected charge carriers [1-3]. In 1963, Pope first reported EL emitted from organic crystals [4]. The efficiency was low, and the driving voltage was up to 400 V. Early organic EL research was mainly focused on anthracene or doped anthracene, tetracene, pyrene and naphthalene crystals [5-10]. However, it was impractical to use organic EL device made from such materials to fabricate displays due to the high operating voltage required to drive such thick EL specimen [11-14]. The ultra-high bias voltage also limits the device power efficiency and hindered organic EL devices from being commercialized.

A high efficiency organic EL diode adopting a double-layered structure invented by Tang from Eastman Kodak in 1987 significantly reduced driving voltage [15]. The double-layered composed of hole-transporting layer and emissive layer was deposited on the indium tin oxide (ITO) coated glass substrate under vacuum, and helped to balance the injection of electrons and holes to improve efficiency. Adachi further added an electron transporting layer between the cathode and the emitting layer to improve device efficiency [16].

## 1.2 Light emitting diodes

Light emitting diodes (LEDs) are designed to convert electricity into light, most of which

are visible to the human eyes. Inorganic LEDs (ILEDs) are usually made through metal-organic chemical vapor deposition on an III-V epitaxial substrate. The main drawbacks of ILEDs are that silicon substrate limited ILEDs from being fabricated into large areas; metal-organic chemical precursor materials usage is huge, and usually those materials are toxic. The crystal orientation determines the spatial distribution of the emitted light. And thus only single color emission can be achieved through ILEDs, which keeps the usage away from a full-color display.

Organic LEDs (OLEDs), on the other hand, can be fabricated into large area. Field-assisted thermionic emission and/or tunneling helps the charge injection in polymer LEDs (PLEDs). The injection is sensitive to the barrier height at the interface of electrode and polymer [17]. Using a high work function anode and a low work function metal cathode would help to facilitate efficient charge injection. The active layer is usually extremely thin (~100nm) so that maximum electrical field and series resistance reduction could be realized. The usage of the ultra-thin active layer with large work function difference electrodes helps to obtain higher EL efficiency. Small molecules OLEDs (SMOLEDs) have a reported power efficiency approximately 100 lm/W, the power efficiency of which exceeded the performance of fluorescent light bulbs [18]. However, high vacuum is required to deposit each layer onto the substrate in SMOLEDs. PLEDs can be solution processed, which reduces the fabrication cost and device size can be varied [15, 19-21]. Contrary to the rigid nature of inorganic electronics, PLEDs can be made flexible [22].

Most of the conjugated polymers or their precursors are soluble in organic solvents, and a high quality thin film can be achieved through solution process. Processing techniques such as spin casting, screen printing or ink-jet printing can be employed to prepare large area displays

with low material consumption and at low cost. The simple fabrication process spurs the interest to develop devices with conjugated polymers. However, the ultra-thin film is prone to defects, such as pinholes [23]. The device efficiency could also be sacrificed if the film is too thin due to the insufficient exciton generation. The optimized multilayer PLED structure by consecutive solution coating also puts severe challenges on the film quality since solvent coating of a new layer must not destroy previous layer(s). Using orthogonal solvents would be one way to resolve the aforementioned issue. Poly(3,4-ethylenedioxythiophene): polystyrene sulfonate (PEDOT: PSS) is also used underneath the emissive polymer layer as a protection layer, and also functions as the hole transporting layer [24].

To summarize, although solution process guarantees low fabrication cost in PLEDs, there are several key challenges to be overcome before fully transferred to stretchable devices:

1) Conventionally used transparent electrode, ITO, is brittle. Small tension strain can crack the entire device.
2) Delicate controlled interface engineering in multi-layered structure to achieve high-efficiency OLED leads to high fabrication cost.
3) Encapsulation is required since the low work function metal cathode and electron injection materials are sensitive to oxygen and/or moisture.

### 1.3 Polymer light emitting electrochemical cells (PLECs)

Is it possible to address the challenges in PLEDs? The answer is yes, and it is demonstrated by the so-called polymer light-emitting electrochemical cells (PLECs), first introduced by Pei in 1995 [25]. PLECs employs an electroluminescent layer between cathode and anode

(Figure1.1). PLEC uses a mixture of conjugated polymer and solid electrolytes to form junction during operation [26, 27]. The electrolyte is made from a salt dissolved in an ionic conductor, for instance, lithium trifluoromethane sulfonate (LiTf) in polyethylene oxide (PEO).

PLECs are unique in operating mechanism among polymer light emitting devices. When a bias voltage greater than the band gap of the conjugated polymer is applied, p- and n- type doping would simultaneously happen at the anode and cathode side. The initially formed p- and n-doped front propagates toward each other until a thin layer of intrinsic region is stabilized when all the ionic species are depleted out of this regime. Such *in situ* electrochemical doping effectively removes the charge injection barriers, both the bulk resistance and contact resistance decreases dramatically. As a result, electrons and holes can be injected into the emissive polymer layer efficiently.

Extensive studies have been made to explore PLECs as an alternative method to PLED due to its simple device architecture and ease of fabrication [28-31]. High external quantum efficiency (~4%), as well as low operating voltage (<4V) could be obtained through this idea [32]. Many researchers have contributed great efforts to understand and optimize the performance of LECs during the past 20 years [33-37]. Different colors PLECs have also been made, such as red, blue, green, and white PLECs [38, 39].

### 1.3.1 PLEC operating mechanism

The operation mechanism of PLECs is mainly based on two important semiconducting properties: electroluminescence and electrochemical doping. PLECs have two operating regimes corresponding to $eV<E_g$ and $eV>E_g$, wherein $E_g$ is the energy band gap of the

conjugated polymer and V is the voltage applied to the conjugated polymer [25-27]. The free cations and anions solvated in the neutral PLEC film are randomly distributed before any bias is applied. When the applied voltage is smaller than $E_g$, double layers would be formed near the electrodes, but no redox-dope to the semiconductor occurs. When bias voltage is larger than Eg, holes and electrons are injected from anode and cathode respectively. The salt can be dissociated into anions and cations to facilitate p- and n-type doping to the conjugated polymer. The luminescent polymer is oxidized near the anode and reduced adjacent to the cathode, forming p-doped and n-doped regime. The electronic charge injection is compensated by oppositely charged ionic species throughout the polymer film to maintain electrical neutrality. The electrical field in the intrinsic region rises sharply to afford continuous charge injections from the opposite electrodes, thus expanding the doping region until a p-i-n junction is evolved in the undoped polymer. The doped and highly conductive polymer provides good electrode contacts by removing the energy barriers between the polymer and electrodes while the undoped regime preserves high luminescence for light emission [34]. This p-i-n junction formation effectively reduced the thickness of active layer. However, this p-i-n junction is dynamic in nature. The doped regions tend to relax by internal discharging and ionic redistribution when the bias is removed. A fully relaxed PLEC has a large open-circuit current, so that PLEC can be regarded as a "light-emitting battery" [40].

The p-i-n junction formation is expected to be slow due to the low ionic conductivity in the solid-state devices [41, 42]. The mobile ions will continue to redistribute until reach an electrochemical equilibrium. Once the junction is formed, electroluminescence turns to be a pure electron-hole recombination process. The EL will turn on sharply, creating a low

resistance pathway for charges. When high efficiency EL is observed from the junction, the ion motion becomes less important. Figure1.2 shows the schematic of EL process in a typical LEC device.

### 1.3.2 Advantages of PLECs

Most of the PLEC devices are turned on at a low voltage (usually no more than 4V) near the energy band gap of the luminescent semiconductor materials [43]. PLECs produce high EL quantum efficiency under both forward and reverse bias [44]. Such "bipolar" behavior has been widely observed. The electrochemical p- and n-doping occurs at the same time and is well balanced: the numbers of electrons and holes injected should be the same. As a result, EL quantum efficiency is high. The combination of low voltage and high EL quantum efficiency gives high power conversation efficiency in PLECs.

The contact between electrode and polymer in PLECs is Ohmic contact as a result of the electrochemical doping. The charge injection in PLECs does not rely on the work function of the electrodes and thus broaden the option for electrode materials. High work function cathode such as aluminum or gold could be readily used to obtain efficient and balanced charge injection. In comparison, a high work function cathode may prohibit the electron injection in PLED by the large energy barrier offset at the polymer and electrode interface [45]. Moreover, the electrochemical doping to the polymer layer makes the contact between the electrode and polymer more conductive, and thus the current flow and the EL turn-on voltage is independent of the work function of the electrode in the PLEC [46].

The formation of the p-i-n junction reduces the effective thickness of the emissive layer,

and thus a thick electroluminescence layer can be adopted in PLECs. Such thick layer is tolerant to a certain degree of non-uniformity and defects in the organic layer. Based on this thickness insensitive feature, planar PLECs are fabricated with two electrodes on top of the EL active layer. The inter-electrode distance can be as large as tens of micrometers [47, 48]. Planar PLECs are insensitive to pinholes or the variation of thickness over the polymer film [40, 49-52]. Planar PLEC device allows direct imaging and scanning techniques to study the p-i-n junction formation mechanism, such as optical beam induced current [51]. Matyba used scanning Kelvin probe microscopy to measure the electrostatic potential within the electroluminescent layer at steady state, and concluded that a majority potential drop happened within the intrinsic junction regime [53].

### 1.3.3 Disadvantages of PLECs

The sluggish ion transportation in the solid state is responsible for the slow diffusion rate during junction formation to reach steady state, and thus PLEC shows a slow response speed. Pre-biasing history would result in the imprecise of the turn-on response [54]. A fast scan rate results in a lower current density and higher EL turn-on voltage [6, 23, 39, 55, 56].

The lifetime of PLECs is short compared to other electroluminescent devices such as PLEDs. The degradation in PLECs usually originates from excessive electrochemical reaction. The electrochemical doping in cathode and anode side starts in a highly diffusive way and needle-like doping fronts were typically observed [57]. Since the advancing speed of p- and n-doped front is not identical, the profile of p-i-n junction is not symmetrically distributed in the center of emissive layer. Needle-shaped doping fronts advance fast, and can protrude all the

way into oppositely doped regime or even reach the opposite electrodes. In the other scenario, p- and n-doping front may collide with each other, causing short circuit problem and therefore causing irreversible degradation to the PLEC device [58].

### 1.3.4 Phase separation

The electroluminescent layer is a mixture of electroluminescent polymer, ionic conductor and ionic source. Additives in almost all the PLEC devices consist at least 5 wt%. The non-polar nature of conjugated polymer and polarity in solid electrolyte would unavoidably form a system involving two-component phase separation with the luminescent polymer in one phase and solid electrolyte in the second phase. Xiong studied the white PLEC at different electrolyte loading and concluded that a moderate ratio of ionic conductor and salt would lead to higher efficiency and longer lifetime [59]. The phase separation appears to cumber the initial electrochemical doping, and may also degrade the device in the junction formation by doping polymers. Ideally, a bicontinuous network is desirable, since the conjugated polymer network provides the pathways for charge transportation, while the electrolyte furnishes channels to transfer ions. Ions must be able to move into conjugated polymer to successfully create the p-i-n junction by electrochemical doping. Cao admixed a bi-functional additive (Figure 1.3a) with the emissive polymer to minimize the phase separation and form a bi-continuous network, thus better device performance could be achieved [60]. The additive has a polar functional end group on one side and a long alkyl non-polar chain on the other, which greatly improves the miscibility with both the polar electrolyte and non-polar conjugated polymer.

### 1.3.5 PLEC Materials

The unique PLEC operating mechanism places stringent requirements on each component. The different polarity of electrolyte and polymers makes it hard to find a common solvent. As a result, many conjugated polymers with high PL efficiency may not be used in PLEC.

Conjugated polymer could only be dissolved in nonpolar solvents. The poly (ethylene oxide), or PEO, used in the PLECs is the first and to date, the most studied electrolyte polymer tolerant to a wide range of salts [25, 34]. Crown ethers can form stable complexes with alkali metal cations since the electronegative oxygen would attract cations tightly [61, 62]. The complexes are soluble in nonpolar solvents. Ion salvation leads to the coordination bonds formation. PEO-based electrolytes are mobile for both the cations and anions with sufficient ionic conductivity and electrochemical stability, allowing simultaneously p- and n-doping [63-65].

Ionic liquids are also used as electrolyte in PLECs. The nonvolatile ionic liquids are soluble in organic solvents with conjugated polymers and insoluble in water. Anions and cations are dissociable from each other and are chemically and electrochemically stable. Stephan used a lipophilic ionic liquid, tetrahexylammonium-bis-trifluoro-methyl-sulfonyl imide as the electrolyte to reach high performance PLECs [61, 62, 66].

### 1.3.6 A comparison of PLECs and PLEDs

PLEC devices utilize both the semiconductor properties and the electrochemical redox properties within the material. In PLEC devices, the oxidized and reduced molecules are immobile but the charge carriers could move back and forth between the electrodes. After a

steady state has been reached under a constant bias, all ion transportation stops. On the contrary, PLEDs have no ionic species in the electroluminescent layer to compensate the electronic charges. Table 1.1 is a brief summary of PLECs and PLEDs.

### 1.3.7 Fixed p-i-n junction PLECs

As mentioned earlier, PLECs usually has a long incubation time due to the necessity of junction formation. The in-situ formed p-i-n junction relaxes once the bias is removed. Efforts have been made to get instantaneous light emission. The fundamental concept is to suppress ionic mobility after junction is formed so that the p-i-n junction can be preserved even after bias is removed. The so-called fixed p-i-n junction can be achieved either by reducing the temperature to below glass transition temperature [67], or polymerize the solid electrolyte [68-70].

Ionic conductors such as methacrylate or acrylate oligomers containing multiple unsaturated functional end groups are of interests. The polar nature of such molecules helps to dissolve certain amount of salt, creating a continuous path to conduct p- and n-type dopants. The heat generated from device operation at high current density or the radicals in electrochemical doping could initiate the curing process. Once the methacrylate or acrylate functional groups are crosslinked, the ionic conduction channels are cut off and would be preserved even after external bias is removed. The well-maintained integrity of p-i-n junction guarantees efficient light emission from the undoped intrinsic EL region. In this way, high efficiency and long life time PLECs can be achieved.

Yu used trimethylolpropane trimethacrylate (TMPTMA) to first demonstrate fixed p-i-n

junction PLECs by curing the ionic conductor [70]. Figure 1.4 shows the formation of fixed p-i-n junction in a PLEC comprising from a curable ionic conductor. The PLEC containing a conjugated polymer, alkoxyphenyl substituted poly(1,4-phenylene vinylene), TMPTMA, and LiTf, at a 100:20:5 weight ratio, was initially charged at 12 V to form the junction. The curing of TMPTMA could be initiated by p-i-n junction formation. Idling for 72 h does not change the light emitting intensity, and the diode feature is retained as shown in Figure 1.5.

## 1.4 PLEC-enabled deformable devices

### 1.4.1 Deformable conductive electrodes

Wearable electronic devices have attracted more interest recently. One of the major challenges to fabricate stretchable light emitting devices has been the absence of elastic transparent conductive electrodes (TCEs). A good TCE should combine the properties of high visual transparency, low surface roughness, high stretchability, and good electrical conductivity [71].

ITO has been the omnipresent TCE material for a long time. ITO coating on flexible substrate (i.e., polyethylene terephthalate) has higher sheet resistance than on the glass substrate since high quality ITO coating requires high temperature annealing. The brittle nature of ITO also limits its flexibility [72]. In search to replace ITO, carbon nanotubes (CNTs), graphene, and metallic nanowires are the candidates attracting research interests.

CNTs [73, 74] and graphene [75] can be used as TCEs to fabricate certain electrical devices since carbon based materials have proper mechanical, electrical and optical properties. Stretchable CNTs can be made by depositing CNTs on top of a stretchable medium [76-79].

Hu has shown that ultrathin single wall carbon nanotubes (SWNT) remain its conductivity after 700% elongation [78]. The high tolerance to the deformation of SWNT arises from the high-aspect-ratio of nanotubes that form the network. Limitation of CNT electrodes is mainly on the high sheet resistance of the electrode for certain applications. Besides, the poor bonding force between CNT and polymer would result in incomplete transfer of CNT from releasing substrate, leading to a high degree of surface roughness. The high surface roughness would cause electrical short and efficiency is reduced. The energy offset between the Fermi level of CNTs and the lowest unoccupied molecular orbital of a conjugate polymer is too large to encourage efficient charge transfer, resulting in a low efficiency device. Graphene has emerged as a new solution processable material with high conductivity and transparency [80,81]. The mechanical properties of carbon based material guarantee the flexibility and stretchability using graphene as electrodes [75]. The difficulties in fabrication of high quality pristine graphene films prohibit its application.

Metallic nanowires network exhibit high transparency, high conductivity, mechanical compliancy, and also solution processability. Silver nanowires (AgNWs) have gained remarkable attention thanks to the simple process and high degree of surface smoothness [81-83]. Liang also soldered the nanowires with a thin layer of graphene oxide before transferring the nanowires to be embedded into the soft polymer matrix to further enhance the conductivity during stretching [83]. AgNWs have been used as TCEs for OLEDs [84-86], solar cells [85, 87, 88], and thin film transistors [89,90]. These devices show comparable or even better device performance to devices fabricated on ITO. The transparency and conductivity of AgNWs film can be tunable by controlling the amount of nanowires deposited on the releasing substrate.

The energy barrier between AgNWs and conjugated polymer is lower, which in turn increases the efficiency of optoelectronic devices built on it.

### 1.4.2 Intrinsically stretchable PLECs

Flexible or stretchable electronics have sprung up as the next generation of electronic applications [91, 92]. Stretchability is more challenging since flexible displays may only need to withstand at most 1% strain, while stretchable displays should be able to survive strain greater than 10% [93]. The requirements on stretchable electronics fabrication are that the mechanical compliant and capability of repeated stretching should not cause physical damage. Combining elastic interconnects with rigid discrete ILEDs or OLEDs has been used in stretchable displays manufacture [94-96]. The resultant displays show high stretchability and efficiency (Figure 1.6). These stretchable interconnecting wires provide the elasticity, while the rigid nature of device remains unchanged. These devices may suffer large stress concentration at the interconnection of rigid-soft interface, which would crack the device during repeated deformation.

Yu developed an intrinsically stretchable PLEC, where all the components, including the substrate, electrodes, and the emissive polymer layer are stretchable at high temperature by adopting a layer of SWNT into a shape memory polymer substrate [78]. Such devices could be stretched up to 45% strain with uniform light emission at 70℃, which is also the glass transition temperature of the shape memory substrate. The limited stretchability at room temperature and conductivity from SWNT/polymer composite electrodes impeded the fabrication of stretchable display on such simple PLEC light emitting device architecture. Liang embedded AgNWs in

an elastomeric polyurethane (PUA) matrix to improve PLEC stretchability at room temperature [97], can be stretched to 120% and with uniform and bright light emission.

## 1.5 Research scope of this dissertation

Chapter 1, the current chapter, provides an introduction to polymers light emitting devices, including PLEDs and PLECs, as well as the initiative of studying stretchable devices.

Chapter 2 studies the influence of electrolytes loading concentration on *p-i-n* junction stability, in the aspects of phase morphology and device performance in order to set up a baseline for stretchable PLEC device. The stable *p-i-n* junction performance can be used to study the stretchability of PLECs.

Chapter 3 continues the work in chapter 2 to transfer the baseline recipe from rigid substrate to a stretchable TCE. The PLECs can undergo high deformation (140%) without compromise light emission characteristics. This chapter focuses on explaining how an interpenetrating network (IPN) could enhance the stretchability.

Chapter 4 concentrates on the relationship between the morphology of bulk heterojunction and stretchability of polymer solar cells (OPV). By forming nanometer scale grain size with free volume left behind, OPV can be made stretchable up to 100%.

Finally, Chapter 5 provides a brief summary and an outlook for future research.

## 1.6 Figures

Figure1.1 Cross-sectional view of a typical PLEC.

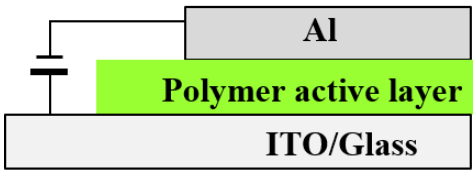

Figure1.2 Electrochemical processes during a PLEC operation. (a) The neutral mixture before applying a voltage, (b, c) n- and p-type doping front formation, and (d, e) charge migration and radiative recombination when a p-i-n junction is formed [Adapted from ref. 29].

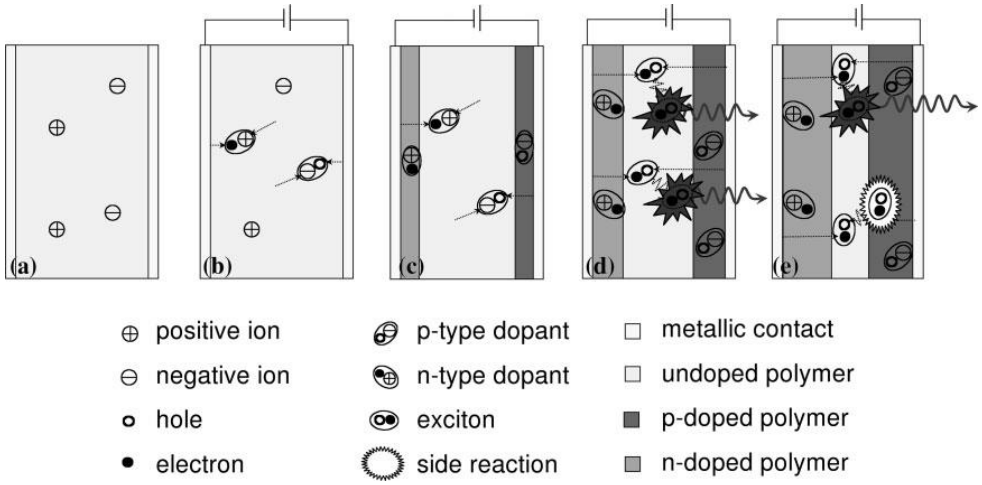

Figure 1.3 Nanoscale phase separation promoted by OCA [Adapted from ref. 60].

(a)

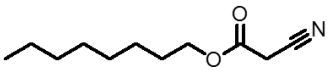


OCA

(b)

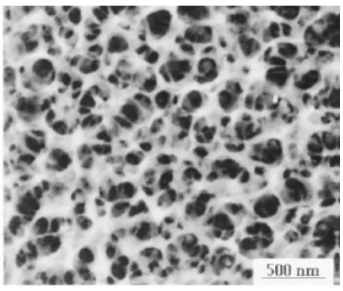

Figure1.4 Fixed p-i-n junction formation initiated by p-i-n junction formation in a PLEC device [Adapted from ref. 70].

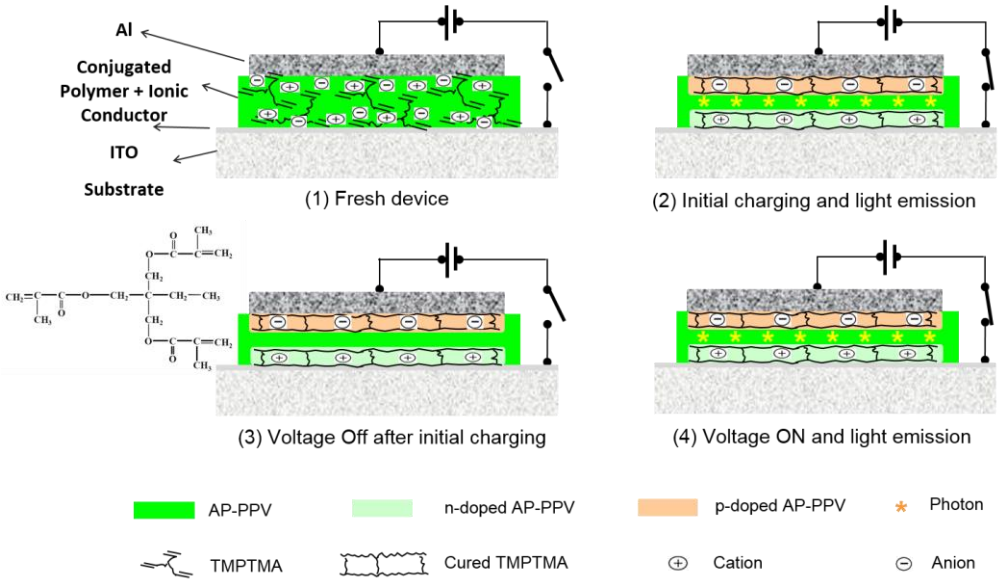

Figure 1.5 Current density and emission intensity response of a fixed p-i-n junction PLEC biased with (a) constant voltage, and (b) pulsed voltage with 50% duty cycle [Adapted from ref. 70].

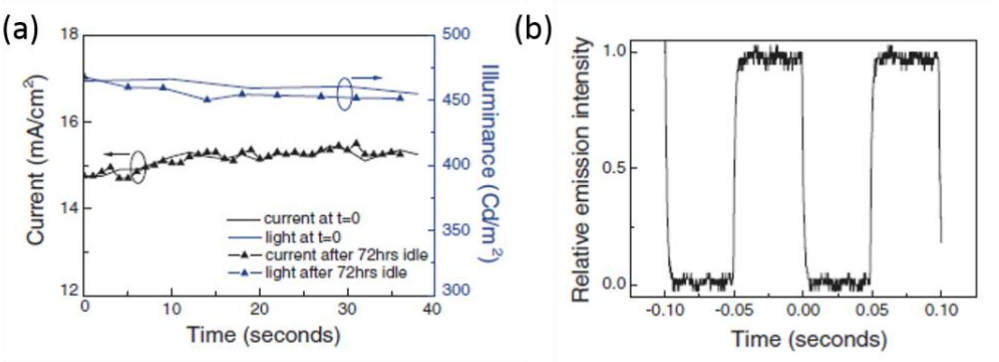

Figure 1.6 A schematic view of ILEDs with serpentine graphene interconnect on a thin PDMS substrate. Optical image of (a) off state, (b, c) on state; (d) Current-voltage measured with different stretching along the horizontal direction [Adapted from ref. 94].

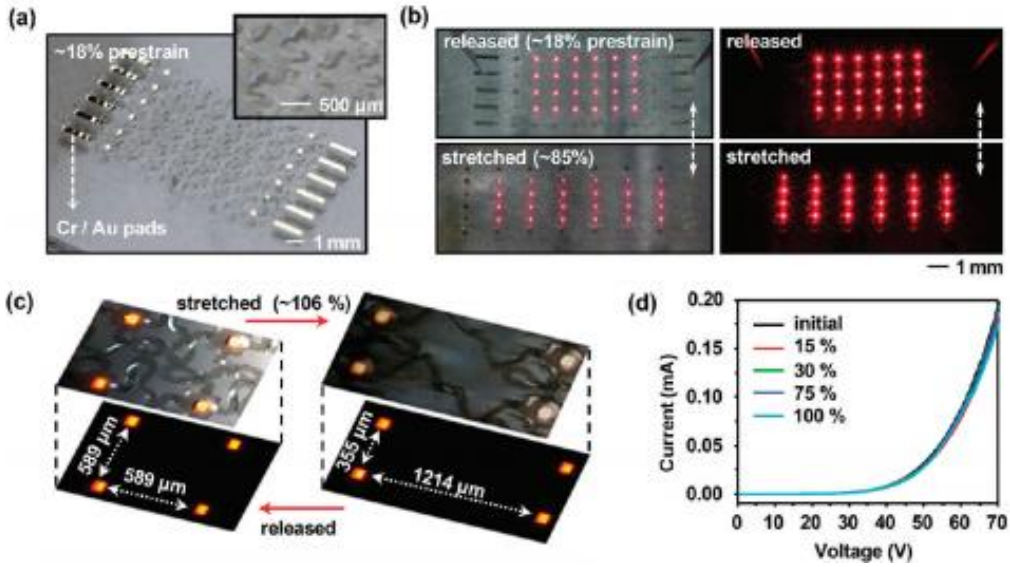

Table 1.1 A comparison between PLECs and PLEDs.

| | PLECs | PLEDs |
|---|---|---|
| Active layer | Conjugated polymer and electrolyte | Conjugated polymers |
| Thickness of active layer | Not sensitive | Thin |
| Anode | Not sensitive | High work-function |
| Cathode | Not sensitive | Low work-function |
| Quantum efficiency | High | Depends on injection balance |
| Operational voltage | Very low | Depends on polymer thickness |
| Response speed | Slow | Fast |

## 1.7 References


1. Schadt, M.; Williams, D .F. Low-temperature hole injection and hole trap distribution in aAnthracenc *J. Chem. Phys.* 1969, *50*, 4364-4367.
2. Williams, D. F.; Schadt, M. DC and pulsed electroluminescence in anthracene and doped anthracene crystals *J. Chem. Phys.* 1970, *53*, 3480-3487.
3. Mehl, W.; Funk, B. Dark injection of electrons and holes and radiative recombination in anthracene with metallic contacts *Phys. Lett. A.* 1967, *25*, 364-365.
4. Pope, M.; Kallmann, H. P.; Magnante, P. Electroluminescence in organic crystals *J. Chem. Phys.* 1963, *38*, 2042.
5. Helfrich, W.; Schneider, W. G. Recombination radiation in anthracene crystals *Phys. Rev. Lett.* 1965, *14*, 229-232.
6. Helfrich, W.; Schneider, W. G. Transients of volume-controlled current and of recombination radiation in anthracene *J. Chem. Phys.* 1966, *44*, 2902.
7. Pott, G. T.; Williams, D. F. Low-temperature Electron injection and space-charge-limited transients in anthracene crystals *J. Chem. Phys.* 1969, *51*, 1901.
8. Lohmann, F.; Mehl, W. Dark injection and radiative recombination of electrons and holes in naphthalene crystals *J. Chem. Phys.* 1969, *50*, 500.
9. Kawabe, M.; Masuyama, A.; Aoki, K.; Masuda, K.; Namba, S. Abnormal laser emission from electron bean excited GaAs *Japan. J. Appl. Phys.* 1970, *9*, 850-851.
10. Wakayama, N. I.; Wakayama, N.; Williams, D. F. Electroluminescence in pentacene doped Anthracene crystals *Bull. Chem. Soc. Jpn.* 1973, *46*, 3395-3399.
11. Wakayama, N. I.; Wakayama, N.; Williams, D. F. Pulsed and steady state

electroluminescence of pentacene doped anthracene crystals *Mol. Cryst. Liq. Cryst.* 1974, *26*, 275-280.

12. Tripathi, G. N. R.; Dubey, D. R.; Padmakar Electroluminescence in doped anthracenc *J. Phys. C: Solid State Phys.* 1977, *10*, 2015-2017.
13. Kalinowski, J.; Godlewski, J.; Signerski, R. Electroluminescence in tetracene crystals *Mol. Cryst. Liq. Cryst.* 1976, *33*, 247-259.
14. Gonzalez Basurto,J.; Burshtein, Z. Electroluminescence studies in pyrene single crystals *Mol. Cryst. Liq. Cryst.* 1975, *31*, 211-217.
15. Tang, C. W.; VanSlyke, S. A. Organic electroluminescent diodes *Appl. Phys. Lett.* 1987, *51*, 913.
16. Adachi, C.; Tokito, S.; Tsutsui, T.; Saito, S. Electroluminescence in organic films with three-layer structure Jpn. J. Appl. Phys. 1988, 2, L269-L271.
17. McGehee, M. D.; Heeger, A. J. Semiconducting (conjugated) polymers as materials for solid-state lasers *Adv. Mater.* 2000, *12*, 1655-1668.
18. Reineke, S.; Lindner, F.; Schwartz, G.; Seidler, N.; Walzer, K.; Lussem, B.; Leo, K. White organic light-emitting diodes with fluorescent tube efficiency *Nature* 2009, *459*, 234-238.
19. Burroughes, J. H.; Bradley, D. D. C.; Brown, A.R.; Marks, R.N.; Mackay, K.; Friend, R. H.; Burn, P. L.; Holmes, A. B. Light-emitting diodes based on conjugated polymers *Nature* 1990, *347*, 539-541.
20. Friend, R. H.; Gymer, R. W.; Holmes, A. B.; Burroughes, J. H.; Marks, R. N.; Taliani, C.; Bradley, D. D. C.; Dos Santos, D. A.; Bredas, J. L.; Logdlund, M.; Salaneck, W. R. Electroluminescence in conjugated polymers *Nature* 1999, *397*, 121-128.

21. Forrest, S. R. The path to ubiquitous and low-cost organic electronic appliances on plastic *Nature* 2004, *428*, 911-918.

22. Gustafsson, G.; Cao, Y.; Treacy, G. M.; Klavetter, F.; Colaneri, N.; Heeger, A. J. Flexible light-emitting-diodes made from soluble conducting polymers *Nature* 1992, *357*, 477-479.

23. Yang, C.; Sun, Q.; Qiao, J.; Li, Y. Ionic liquid doped polymer light-emitting electrochemical cells *J. Phys. Chem. B* 2003, *107*, 12981-12988.

24. Li, G.; Shrotriya, V.; Huang, J.; Yao, Y.; Moriarty, T.; Emery, K.; Yang, Y. High-efficiency solution processable polymer photovoltaic cells by self-organization of polymer blends *Nat. Mater.* 2005, 4, 864 – 868.

25. Pei, Q.; Yu, G.; Zhang, C.; Yang, Y.; Heeger, A. J. Polymer light-emitting electrochemical cells *Science* 1995, *269*, 1086-1088.

26. Dini, D. Electrochemiluminescence from organic emitters *Chem. Mat.* 2005, *17*, 1933-1945.

27. Armstrong, N. R.; Wightman, R. M.; Gross, E. M. Light-emitting electrochemical processes *Ann. Rev. Phys. Chem.* 2001, *52*, 391.

28. Yu, Z.; Wang, M.; Lei, G.; Liu, J.; Li, L.; Pei, Q. Stabilizing the dynamic p-i-n junction in polymer light-emitting electrochemical cells. J. Phys. Chem. Lett. 2011, 2, 367-372.

29. Fang, J.; Matyba, P.; Edman, L. The design and realization of flexible, long-lived light-emitting electrochemical cells Adv. Funct. Mater. 2009, 19, 2671-2676.

30. Graber, S.; Doyle, K.; Neuburger, M.; Housecroft, C. E.; Constable, E. C.; Costa, R. D.; Orti, E.; Repetto, D.; Bolink, H. J. A supramalecularly caged ionic iridium (III) complex yielding bright and very stable solid-state light-emitting electrochemical cells J. Am. Chem. Soc. 2008, 130, 14944-14945.

31. Shao, Y.; Bazan, G. C.; Heeger, A. J. Long-lifetime polymer light-emitting electrochemical cells Adv. Mater. 2007, 19, 365-370.

32. Sun, Q.; Li, Y.; Pei, Q. Polymer light-emitting electrochemical cells for high-efficiency low-voltage electroluminescent devices J. Display Tech. 2007, 3, 211-224.

33. Pei, Q.; Hegger, A. J. Operating mechanism of light-emitting electrochemical cells Nat. Mater. 2008, 7, 167.

34. Pei, Q.; Yang, Y.; Yu, G.; Zhang, C.; Heeger, A. J. Polymer light-emitting electrochemical cells: in situ formation of a light-emitting p-n junction *J. Am. Chem. Soc.* 1996, *118*, 3922-3929.

35. Pei, Q.; Yang, Y.; Yu, G.; Cao, Y.; Heeger, A. J. Solid state polymer light-emitting electrochemical cells: recent developments Synth. Met. 1997, 85, 1229-1232.

36. Yu, Z.; Li, L.; Gao, H.; Pei, Q. Polymer light-emitting electrochemical cells: recent developments to stabilize the p-i-n junction and explore novel device applications. Science China Chemistry, 2013, 56, 1075-1086.

37. Liang, J.; Yu, Z.; Li, L.; Gao, H.; Pei, Q.; Zhao, Y.S. (ed.) *Organic nanophotonics*, nano-optics and Nanophotonics. Chap 4.

38. Yang, Y.; Pei, Q. Voltage controlled two color light-emitting electrochemical cells Appl. Phys. Lett. 1996, 68, 2708.

39. Yang, Y.; Pei, Q. Efficient blue-green and white light-emitting electrochemical cells based on poly[9,9-bis(3,6-dioxaheptyl)-fluorene-2,7-diyl] *J. Appl. Phys.* 1997, *81*, 3294.

40. Gao, J.; Dane, J. Visualization of electrochemical doping and light-emitting junction formation in conjugated polymer films *Appl. Phys. Lett.* 2004, *84*, 2778.

41. Manzanars, J. A.; Reiss, H. Polymer light-emitting electrochemical cells: a theoretical study of junction formation under steady-state conditions *J. Phys. Chem. B* 1998, *102*, 4327-4336.

42. de Mello, J.C.; Tessler, N.; Graham, S. C.; Friend, R. H. Ionic space-charge effects in polymer light-emitting diode *Phys. Rev. B* 1998, *57*, 12951-12963.

43. Brown, T. M.; Kim, J. S.; Friend, R. H.; Cacialli, F.; Daik, R.; Feast, W. J. Built-in field electroabsorption spectroscopy of polymer light-emitting diodes incorporating a doped poly(3,4-ethylene dioxythiophene) hole injection layer *Appl. Phys. Lett.* 1999, *75*, 1679-1681.

44. Cao, Y.; Yu, G.; Zhang, C.; Menon, R.; Heeger, A. J. Polymer light-emitting diodes with polyethylene dioxythiophene-polystyrene sulfonate as the transparent anode *Synth. Met.* 1997, *87*, 171-174.

45. Sun, Q.; Yang, C.; He, G.; Li, Y.; Wang, H. Effects of electrode modifications on the performance of polymer light-emitting electrochemical cells *Synth. Met.* 2003, *138*, 561-565.

46. Kraft, A.; Grimsdale, A. C.; Holmes, A. B. Electroluminescent conjugated polymers—seeing polymers in a new light *Angew. Chem. Int. Ed.* 1998, *37*, 402-408.

47. Shin, J. H.; Dzwilewski, A.; Iwasiewicz, A.; Xiao, S.; Fransson, A.; Ankah, G. N.; Edman, L. Light emission at 5 V from a polymer device with a millimeter-sized interelectrode gap *Appl. Phys. Lett.* 2006, *89*, 013509

48. Cao, Y.; Parker, I. D.; Yu, G.; Zhang, C.; Heeger, A. J. Improved quantum efficiency for electroluminescence in semiconducting polymers *Nature* 1999, *397*, 414-417.

49. Gao, J.; Dane, J. Imaging the doping and electroluminescence in extremely large planar polymer light-emitting electrochemical cells *J. App. Phys.* 2005, *98*, 063513.

50. Hu, Y.; Tracy, C.; Gao, J. High-resolution imaging of electrochemical doping and dedoping process in luminescent conjugated polymers *App. Phys. Lett.* 2006, *88*, 123507.

51. Dick, D. J.; Heeger, A. J.; Yang, Y.; Pei, Q. Imaging the structure of the p-n junction in polymer light-emitting electrochemical cells *Adv. Mater.* 1996, *8*, 985-987.

52. Yu, G.; Pei, Q.; Heeger, A. J. Planar light-emitting devices fabricated with luminescent electrochemical polyblends *Appl. Phys. Lett.* 1997, *70*, 934.

53. Matyba, P.; Maturova, K.; Kemerink, M.; Robinson, N. D.; Edman, L. The dynamic organic p-n junction Nat. Mater. 2009, 8, 672-676.

54. Sun, Q. J.; Zhan, X. W.; Zhang, B.; Yang, C. H.; Liu, Y. Q.; Li, Y. F.; Zhu, D. B. Polymer light-emitting electrochemical cell based on a novel poly(aryleneethynylene) consisting of ethynylfluorene and tetraphenyldiaminobiphenyl units *Polym. Adv. Technol.* 2004, *15*, 70.

55. Ho, G. K.; Meng, H. F.; Lin, S. C.; Horng, S. F.; Hsu, C. S.; Chen, L. C.; Chang, S. M. Efficient white light emission in conjugated polymer homojunctions *Appl. Phys. Lett.* 2004, *85*, 4576.

56. Xu, Y. H.; Peng, J. B.; Cao, Y. Efficient polymer white-light-emitting diodes *Appl. Phys. Lett.* 2005, *86*, 163502.

57. Shin, J. H.; Xiao, S.; Edman, L. Polymer light-emitting electrochemical cells: The formation and effects of doping-induced micro shorts Adv. Funct. Mater. 2006, 16, 949-956.

58. Wagberg, T.; Hania, P. R.; Robinson, N. D.; Shin, J. H.; Matyba, P.; Edman, L. On the

limited operational lifetime of light-emitting electrochemical cells Adv. Mater. 2008, 20, 1744-1749.

59. Xiong, Y.; Li, L.; Liang, J.; Gao, H.; Chou, S.; Pei, Q. Efficient white polymer light-emitting electrochemical cells Mater. Horiz. 2015, 2, 338-343.
60. Cao, Y.; Yu, G.; Heeger, A. J. Efficient, fast response light-emitting electrochemical cells: electroluminescent and solid electrolyte polymers with interpenetrating network morphology Appl. Phys. Lett. 1996, 68, 3218-3220.
61. Cao, Y.; Pei, Q.; Andersson, M. R.; Yu, G.; Heeger, A. J. Light-emitting electrochemical cells with crown ether as solid electrolyte J. Electrochem. Soc. 1997, 144, L317-L320.
62. Collie, L.; Parker, D.; Tachon, C.; Hubbard, H. V. S.; Davies, G. R.; Ward, I. M.; Wellings, S. C. Synthesis and lithium transport in ionically conducting crown-ether polymers Polymer 1993, 34, 1541-1543.
63. Sun, Q.; Wang, H.; Yang, C.; He, G.; Li, Y. Blue-green light-emission LECs based on block copolymers containing di(a-naphthalene vinylene) benzene chromophores and tri(ethylene oxide) spacers *Synth. Met.* 2002, *128*, 161-165.
64. Sun, Q.; Wang, H.; Yang, C.; Li, Y. Synthesis and electroluminescence of novel copolymers containing crown ether spacers *J. Mat. Chem.* 2003, *13*, 800-806.
65. Sun, Q.; Wang, H.; Yang, C.; Wang, X.; Liu, D.; Li, Y. Polymer light-emitting electromical cells with the block copolymers containing PEO segments *Thin Sol. Films* 2002, *417*, 14-19.
66. Panozzo, S.; Armand, M.; Stephan, O. Light-emitting electrochemical cells using a molten delocalized salt Appl. Phys. Lett. 2002, 80, 679-681.

67. Yu, G.; Cao, Y.; Andersson, M.; Gao, J.; Heeger, A. J. Polymer light-emitting electrochemical cells with frozen p-i-n junction at room temperature Adv. Mater. 1998, 10, 385-388.

68. Leger, J. M.; Rodovsky, D. B.; Bartholomew, G. P. Self-assembled, chemically fixed homojunctions in semiconducting polymers Adv. Mater. 2006, 18, 3130-3134.

69. Leger, J. M.; Patel, D. G.; Rodovsky, D. B.; Bartholomew, G. P. Polymer photovoltaic devices employing a chemically fixed p-i-n junction Adv. Funct. Mater. 2008, 18, 1212-1219.

70. Yu, Z.; Sun, M.; Pei, Q. Electrochemical formation of stable p-i-n junction in conjugated polymer thin films J. Phys. Chem. B 2009, 113, 8481-8486.

71. Cairns, D. R.; Witte, R. P.; Sparacin, D. K.; Sachsman, S. M.; Paine, D. C.; Crawford, G. P.; Newton, R. R. Strain-dependent electrical resistance of tin-doped indium oxide on polymer substrates Appl. Phys. Lett. 2000, 76, 1425-1427.

72. Geim, A. K. Graphene: status and prospects Science 324, 2009, 1530-1534.

73. Rowell, M. W.; Topinka, M. A.; McGehee, M. D.; Prall, H. J.; Dennler, G.; Sariciftci, N. S.; Hu, L.; Gruner, G. Organic solar cells with carbon nanotube network electrodes Appl. Phys. Lett. 2006, 88, 233506.

74. Zhang, D.; Ryu, K.; Liu, X.; Polikarpov, E.; Ly, J.; Tompson, M. E.; Zhou, C. Transparent, conductive and flexible carbon nanotube films and their application in organic light-emitting diodes Nano Lett. 2006, 6, 1880-1886.

75. Kim, K. S.; Zhao, Y.; Jang, H.; Lee, S. Y.; Kim, J. M.; Kim, K. S.; Ahn, J. H.; Kim, P.; Choi, J. Y.; Hong, B. H. Large-scale pattern growth of graphene films for stretchable transparent

electrodes Nature 2009, 457, 706-710.

76. Yuan, W.; Hu, L.; Yu, Z.; Lam, T.; Biggs, J.; Ha, S. M.; Xi, D.; Chen, B.; Senesky, M. K.; Gruner, G.; Pei, Q. Fault-tolerant dielectric elastomer actuators using single-walled carbon nanotube electrodes Adv. Mater. 2008, 20, 621-625.
77. Brochu, P.; Stoyanov, H.; Chang, R.; Niu, X.; Hu, W.; Pei, Q. Capacitive energy harvesting using highly stretchable silicone-carbon nanotube composite electrodes Adv. Energy Mater. 2014, 4, 1300659.
78. Hu, L.; Yuan, W.; Brochu P.; Gruner, G.; Pei, Q. Highly stretchable, conductive, and transparent nanotube thin films Appl. Phys. Lett. 2009, 94, 161108.
79. Yu, Z.; Niu, X.; Liu, Z.; Pei, Q. Intrinsically stretchable polymer light-emitting devices using carbon nanotube-polymer composite electrodes Adv. Mater. 2011, 23, 3989-3994.
80. Novoselov, K. S.; Geim, A. K.; Morozov, S. V.; Jiang, D.; Zhang, Y.; Dubonos, S. V.; Grigorieva, I. V.; Firsov, A. A. Electric field effect in atomically thin carbon films Science 2004, 306, 666-669.
81. Yu, Z.; Li, L.; Zhang, Q.; Hu, W.; Pei, Q. Silver nanowire-polymer composite electrodes for efficient polymer solar cells Adv. Mater. 2011, 23, 4453-4457.
82. Yu, Z.; Zhang, Q.; Li, L.; Chen, Q.; Niu, X.; Liu, J.; Pei, Q. Highly flexible silver nanowire electrodes for shape-memory polymer light-emitting diodes Adv. Mater. 2011, 23, 664-668.
83. Li, L.; Yu, Z.; Hu, W.; Chang, C. H.; Chen, Q.; Pei, Q. Efficient flexible phosphorescent polymer light-emitting diodes based on silver nanowire-polymer composite electrode Adv. Mater. 2011, 23, 5563-4467.
84. Zeng, X.Y.; Zhang, Q. K.; Yu, R. M.; Lu, C. Z. A new transparent conductor: silver

nanowire film buried at the surface of a transparent polymer Adv. Mater. 2010, 22, 4484-4488.

85. Langley, D.; Giusti, G.; Mayousse, C.; Celle, C.; Bellet, D.; Simonato, J. P. Flexible transparent conductive materials based on silver nanowire networks: a review Nanotechnology 2013, 24, 452001.

86. Lee, Y.; Suh, M.; Kim, D.; Lee, D.; Chang, H.; Lee, H. S.; Kim, Y. W.; Kim, T.; Suh, K. S.; Jeon, D. Y. Improved operational stability of polymer light-emitting diodes based on silver nanowire electrode through pre-bias conditioning treatment Adv. Funct. Mater. 2014, 24, 6465-6472.

87. Song, M.; Park, J. H.; Kim, C. S.; Kim, D. H.; Kang, Y. C.; Jin, S. H.; Jin, W. Y.; Kang, J. W. Highly flexible and transparent conducting silver nanowire/ZnO composite film for organic solar cells Nano Res. 2014, 7, 1370-1379.

88. Jin, J.; Lee, J.; Jeong, S.; Yang, S.; Ko, J. H.; Im, H. G.; Baek, S.W.; Lee, J. Y.; Bae, B. S. High-performance hybrid plastic films: a robust electrode platform for thin-film optoelectronics energy Environ. Sci. 2013, 6, 1811-1817.

89. Yu, C. H.; Wu, H. C.; Chien, C. Effect of passivation layer on InGaZnO thin-film transistors with hybrid silver nanowires as source and drain electrodes Jpn. J. Appl. Phys. 2015, 54, 081101.

90. Liu, H. C.; Lai, Y. C.; Lai, C. C.; Wu, B. S.; Zan, H. W.; Yu, P.; Chueh, Y. L.; Tsai, C. C. Highly effective field-effect mobility amorphous InGaZnO TFT mediated by directional silver nanowire arrays ACS Appl. Mater. Interfaces 2015, 7, 232-240.

91. Filiatrault, H. L.; Porteous, G. C.; Carmichael, R. S.; Davidson, G. J. E.; Carmichael, T. B.

Stretchable light-emitting electrochemical cells using an elastomeric emissive material Adv. Mater. 2012, 24, 2673-2678.

92. Someya, T. Flexible electronics: tiny lamps to illuminate the body Nat. Mater. 2010, 9, 879-880.
93. Vosgueritchian, M.; Tok, J. B. H.; Bao, Z. Stretchable LEDs: Light-emitting electronic skins Nat. Photonics *2013*, 7, 769-771.
94. Kim, R. H. et al., Stretchable, transparent graphene interconnects for arrays of microscale inorganic light emitting diodes on rubber substrates Nano Lett. 2011, 11, 3881-3886.
95. Park, S. I. et al. Printed assemblies of inorganic light-emitting diodes for deformable and semitransparent displays Science 2009, 325, 977-981.
96. Sekitani, T.; Nakajima, H.; Maeda, H.; Fukushima, T.; Aida, T.; Hata, K.; Someya, T. Stretchable active-matrix organic light-emitting diode display using printable elastic conductors Nat. Mater. 2009, 8, 494-499.
97. Liang, J; Li, L.; Niu, X.; Yu, Z.; Pei, Q. Elastomeric polymer light-emitting Devices and displays Nat. Photonics 2013, 7, 817-824.

## Chapter 2 Efficient polymer light emitting electrochemical cells

### 2.1 Introduction

Polymer light emitting electrochemical cells (PLECs) were first introduced in 1995 [1]. The mixture of conjugated polymer with salt and ionic conductor serves as the active layer and is sandwiched between the anode and the cathode. Voltage required to form a dynamic p-i-n junction is equal to or larger than the band gap of the electroluminescent polymer [2, 3]. The dynamic junction is formed when p- and n-doped region at anode and cathode propagate towards each other. The junction formation enhances charge carrier injection by reducing the charge injection barrier height and thus improves the recombination of electrons and holes, and thus allows the usage of a high work function cathode. It has been demonstrated that PLECs have low turn-on voltage, long lifetime and high efficiency at a relatively low current density and/or brightness [4-7].

The intrinsic regime is usually closer to the cathode side and shrinks in size during constant current stressing test [8]. The shift in the intrinsic junction indicates that the electrochemical reactions are still underway and not cut off after the junction formation. Possible explanations are: 1) the cations and anions in the intrinsic region can move back and forth via thermally activated diffusion process and contribute to the electrochemically doping propagation and, 2) a highly doped conjugated polymer could transfer their dopants into the intrinsic area via excessive oxidation or reduction doping. The reduced photoluminescence and short lifetime in PLECs can be attributed to such excessive electrochemical reaction [9-17]. Crosslinked doping front helps to prevent excessive extension into the intrinsic regime, which is also known as the

fixed p-i-n junction PLECs [17-19]. The polymerized buffer layer confines ion mobility and prevents the as formed p- and n-doped region from relaxation, thus fast response and longer lifetime is achievable [5, 20-24].

Phase separation would also influence PLEC performance in the aspect of lifetime and photoluminescence. The polar nature of electrolyte and non-polar nature of conjugated polymer leaves phase separation unavoidable. In this chapter, my work focused on studying the impact of different electrolyte loading concentration on phase morphology and PLEC device performance.

Alkoxyphenyl substituted poly(1,4-phenylene vinylene) (SY-PPV, Super-Yellow by Merck) is a yellow color emitting polymer [25,26]. It is chosen to be a model compound of light emitting polymer owing to its solubility in common organic solvents, high photoluminescence (PL) and electroluminescence (EL) quantum yields [5, 22, 27-30]. Ionic conductors used here are SR10 and ETPTA (Figure 2.1b and c), with molecular weight at 1000 g/mol. Ionic conductors with different polyethylene oxide (PEO) length and different end encapsulation groups can interfere with the PLECs performance, since the PEO segments can provide competent ionic conductivity for electrochemical reactions in the p-i-n junction formation and the functional end groups participate in forming a fixed p-i-n junction. PLEC devices are made with a relatively simple three-layer sandwiched structure: indium tin oxide (ITO)/ electroluminescent layer/ aluminum (Al), with ITO wired to the anode and Al to the cathode.

## 2.2 Experimental methods

***Sample preparation.*** A 15Ω/□ surface sheet resistance ITO glass substrate was ultrasonically cleaned for 30 minutes each, using detergent water, deionized water, acetone, and isopropanol. SY-PPV, ionic conductors, and LiTf salt were dissolved separately at room temperature in anhydrous, inhibitor-free tetrahydrofuran (THF). The solutions were mixed at different weight ratio and the final SY-PPV master solutions' concentration was 8 mg/mL. For convenience, the weight ratios are all referring to the SY-PPV. The solution mixture was spin-coated directly onto ITO substrates at 2000 rpm inside the glove box. The samples were stored in vacuum at room temperature for 30 minutes to remove the residual THF solvent in the active layer. An aluminum top electrode, 80 nm thick, was deposited using an electron-beam metal evaporation system at $3\times10^{-6}$ torr. A shadow mask was used to define the device area as 12 $mm^2$.

***Characterization.*** Current-voltage response measurements were conducted in the nitrogen-protected dry box. Keithley 2400 source-meter was used to record the current-voltage (I-V) curve. Atomic force microscope (AFM) was carried out on a Bruker dimension icon scanning probe microscope at ambient conditions.

## 2.3 Results and discussion

### 2.3.1 Influence of different ionic conductors

Poly(ethylene oxide) (PEO) was widely used as ionic conductor due to its high ionic conductivity and high-quality film forming capability. However, the hydrophilic and strong polarity puts a rigorous selection of a proper solvent to dissolve everything into homogeneous solution. Different ionic conductors in replacement of PEO have been studied to achieve fast

turn-on speed, long lifetime, or high luminescent. A polymer film containing SY-PPV, 10 wt% of ionic conductor (ETPTA or SR10) and 5 wt% of LiTf salt with thickness around 200 nm was spin-casted onto an ITO glass substrate. Figure 2.2 reveals the light emission evolution over time for PLEC devices using different ionic conductors driven at constant 3 mA current and 10 V voltage compliance.

The distinctive structures of SR10 and ETPTA may be responsible for the different turn-on speed and brightness. SR10 incorporates ionic conduction ethylene oxide blocks next to each curable methacrylate functional termination group on both ends. ETPTA, on the other hand, is a branched structure with acrylate group encapsulated at the three branched chain ends. Although ETPTA has more pathways to conduct ions, it has high probability for ions to hop back and forth, thus it may take longer time to reach an equilibrium state. PLEC device using SR10 has a brightness up to $1.6\times10^3$ cd/m$^2$ with 6.5 cd/A current efficiency. The brightness reaches $1.8\times10^3$ cd/m$^2$ in the ETPTA incorporated PLEC device, and the current efficiency is 7.3cd/, representing a 12.5% enhancement over PLEC using SR10. The turn-on time for the PLEC device with ETPTA is three times lower than the device using SR10. Although fast turn-on speed indicates a high conductivity, low ionic mobility would help to obtain a smooth propagation p- and n-doping front interface with the intrinsic area. [7] PLEC device using ETPTA as ionic conductor has a longer lifetime and is more stable in the stressing test. Since a fixed p-i-n junction can be formed through initial p-i-n junction formation [22], we can pre-charge pristine PLEC with moderate stressing force to form a fixed p-i-n junction in PLEC device to guarantee immediate turn on in the following operation. Considering its better lifetime and higher brightness, ETPTA is then used as a strategy to help understand the

relationship of loading concentration and device performance.

### 2.3.2 Influence of solid electrolyte concentration on PLEC performance

Previous research showed the influence of ion concentration on the PLEC operating time [6, 10, 31-33]. The salt concentration in PLECs can be varied in a wide range to impart the electroluminescence properties by providing ions in the p-i-n junction formation and charge transportation. Excessive salt and ionic conductor could cause severe phase separation, and thus disturb the pathway formation or raise the stability issue induced by side-reaction in the p-i-n junction degradation during PLEC operation. A series of different electrolyte loading concentration have been studied in the aspects of phase morphology and device performance to set up the recipe baseline for a stretchable PLEC.

ETPTA has quite low molecular weight (1000 g/mol) with low vapor pressure [3, 34-37]. Although it may be volatile in high vacuum and under high temperature during aluminum electrode deposition, Fourier Transform Infrared (FTIR) measurements indicated no absorption intensity difference before and after thermal evaporation at 1728 $cm^{-1}$ in SY-PPV:ETPTA:LiTf upon high vacuum and temperature process as shown in Figure 2.3. The majority of the ionic conductor still remained by the strong absorption at featured wavelength at 1728 $cm^{-1}$, which is the fingerprint of the vibronic motion of the carbonyl groups in the acrylate groups. However, the sample should not be overheated in top electrode thermal deposition, which could lead to major loss of small molecules [38].

The sandwiched PLEC device was biased at 3mA with 10V compliance voltage. The weight ratio of the spin-casted films being studied is listed in Table 2.1. All the PLEC devices

were biased under constant 3 mA current source with 10V compliance voltage.

The temporal evolution of luminous for different loading concentrations of salt (1-10%) and an ionic conductor (10-20%) is shown in Figure 2.4a. The initial current is contributed by the ionic redistribution within the active layer when an electric field is applied, and therefore luminance is low at first. The turning points on the luminance curves where platform appears indicate the change of driving mode from constant voltage to constant current. The PLEC device responded faster with higher concentration of ionic conductor or ions since more ionic pathway and dopants are readily to be used to dope the polymer to effectively reduce the junction thickness and emit light. The response speed (turn-on speed) is roughly determined by the time required to reach 90% of its maximum emission brightness [20]. With the same amount of ion concentration (4 wt%), sample 5 has the fastest turn-on speed. With the same ionic conductor concentration in the active layer (10 wt%), the turn-on speed is faster with increasing ion loading concentration.

Sample 5 exhibits fast increase in brightness at the first 3 min to peak brightness at 1100 $cd/m^2$ and decay to 900 $cd/m^2$ within 10 minutes. When the ionic conductor concentration is more than 20%, quenching phenomenon may start to hinder the PLEC performance and result in decreasing brightness and efficiency. From the luminescence vs. time curve in sample 1, the brightness value increases at the very beginning due to the p-i-n junction formation; and decreases gently after reaching its maximum brightness. We speculate that the decrease is caused by the lack of ion source. The shortage of dissociable ion source to build up an ideal doping profile might cause the ions to move back and forth from the doped regions into the intrinsic region, thus decrease the device stability. As indicated in Figure 2.4a, the best

brightness performance is obtained with a loading ratio of 15% ETPTA and 4% LiTf (Sample 4). The same device exhibits the longest lifetime. The intermediate PEO segments in ETPTA provide sufficiently ionic conductivity for the junction formation; and crosslinking reaction could be initiated to polymerize the acrylate end group which then confines the movement of ionic species and dopants in the emissive polymer layer. The development of localized doping front effectively prevents the extrusion of doping fronts and preserves the integrity of a p-i-n junction during the whole operation time frame. Fixed p-i-n junction formation also helps to suppress electrochemical overreactions. Table 2.2 summarized PLEC device performance with different loading concentration.

To further understand the relationship of electrolyte loading concentration and EL behavior, tapping mode atomic force microscope (AFM) is used to study the phase morphology of above mentioned PLEC active layers (Figure 2.5). No significant morphology difference was observed among the use of ion salt within 4%. Increasing the salt concentration to 10%, a poor compatibility between the polar moieties (ion-transporting medium and salt) and the hydrophobic host conjugated polymer is formed in Figure 2.5c. Macroscopic phase separation having large domains with higher loading concentrations [39], and in turn, severely lessens the brightness and lifetime of the PLECs even though the junction incubation period is reduced.

Shoji reported that improved brightness could be achieved by higher concentration of salt [40]. The results in this work exhibit that when the salt concentration is too small (1%), there is no sufficient ion source to completely form the junction, although a faster turn-on speed and current efficiency is accompanied. Increasing the salt concentration and ionic conductor concentration moderately could redistribute ions for a better p-i-n junction formation. The

electroluminescence keeps increasing with a higher salt concentration when keeping all other parameters the same. When the salt concentration is higher than 10%, phase separation is unavoidable.

Edman pointed out the trade-off between fast response and long lifetime as well [41]. In this SY-PPV system, 1% salt device turns on fast and is fairly stable, but has a low electroluminescence. The 4% salt devices have moderate turn on speed with high brightness when ionic conductor concentration is increased. The lifetime of the PLEC with 15% ionic conductor and 4% LiTf displayed brightness of ~1500 cd/m$^2$ without any sign of degradation during 15h operation under 3mA constant current driving. Therefore, we choose the ratio of ETPTA at 15 wt%, and LiTf at 4 wt% as the baseline for further studies.

### 2.3.3 PLEC device with dual ionic conductors

PEO is a traditionally used ionic conductor despite the fact that it addresses rigorous phase separation in the PLEC mixture with polymer and salts. The high molecular weight PEO would greatly reduce its solubility in the conjugated polymer. However, its low glass transition temperature and lack of crosslinkable end groups are of interest as a soft medium to accommodate large strain applied to the active layer.

The highest brightness is 1000 cd/m$^2$ and 800 cd/m$^2$ in the device with 15 wt% and 25 wt% PEO (Figure 2.6). In both devices, PLEC shows photoluminescence reduction. The hydroxyl end group on PEO chain may be activated during doping and negatively affect the electrochemical oxidation or reduction which causes destruction within the PLECs permanently.

AFM shows severe phase separation in PLEC using a combination of PEO and ETPTA as ionic conductors (Figure 2.7), which might block the ions conductivity from chain to chain for electrochemical doping. Active layer with 25 wt% PEO has a larger phase separation dimension which explains the poor EL and device stability. Although using 15 wt% PEO in the PLEC still shows phase separation, the existence of PEO would enhance the stretchability of emissive layer, and this SY-PPV:ETPTA:PEO:LiTf (weight ratio of 100:15:15:4) is used as baseline recipe for stretchable PLEC study.

## 2.4 Summary

To summarize, we have demonstrated high electroluminescence and moderate lifetime PLECs by investigating the influence of electrolyte loading concentration and their morphology. A baseline recipe for stretchable PLEC is set, using SY-PPV:ETPTA:PEO:LiTf at weight ratio of 100:15:15:4. This PLEC could reach ~1000 cd/m$^2$ luminescence in a short time and can perform relatively stable for 1h before luminance decreased to 90%. Ionic conductor with curable acrylate end group enhances the lifetime and efficiency of PLEC by forming fixed p-i-n junction. Increasing the amount of salt would rise severe phase separation concern. Although the incorporation of PEO causes unavoidable phase separation, it brings the possibility to achieve stretchability in the otherwise non-stretchable film.

## 2.5 Figures

Figure 2.1 Chemical structural of (a) SY-PPV, (b) SR10, and (c) ETPTA.

(a)

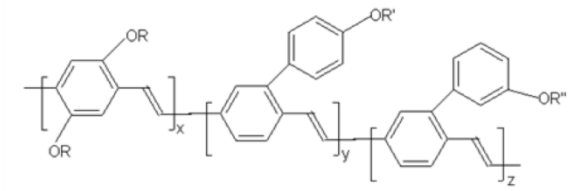


(b)

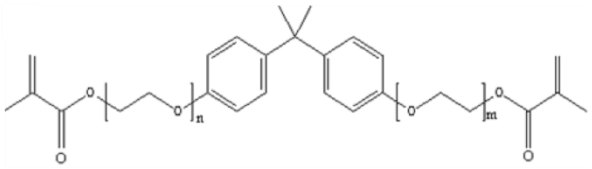


(c)

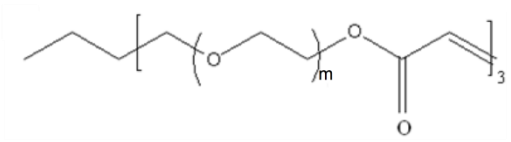

Figure 2.2 Brightness vs. time (a) and efficiency vs. time (b) of a PLEC device operating at 10 V. The emissive layer is SY-PPV: SR10: LiTf and SY-PPV: ETPTA: LiTf (100:10:5 by weight).

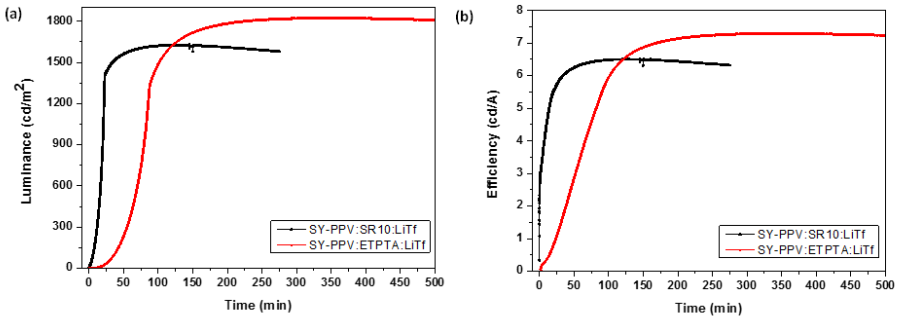

Figure 2.3 FTIR spectra for a composite film with SY-PPV, 10% ETPTA and 4% LiTf before and after the high vacuum aluminum electrode deposition.

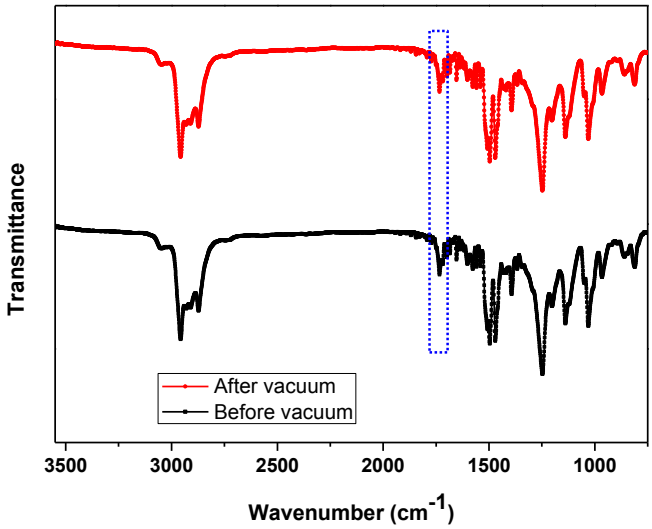

Figure 2.4 PLEC stressing test of (a) Luminance vs. time, and (b) Efficiency vs. time at a constant 3 mA current source.

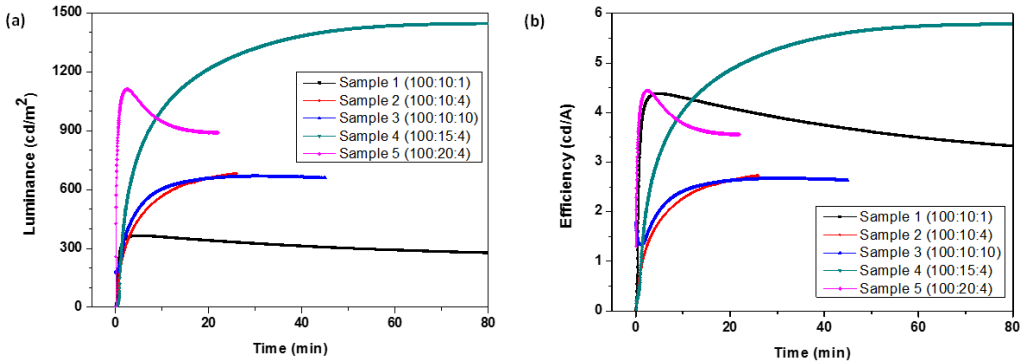

Figure 2.5 AFM phase images of (a) sample 1, (b) sample 2, (c) sample 3, (d) sample 4, (e) sample 5.

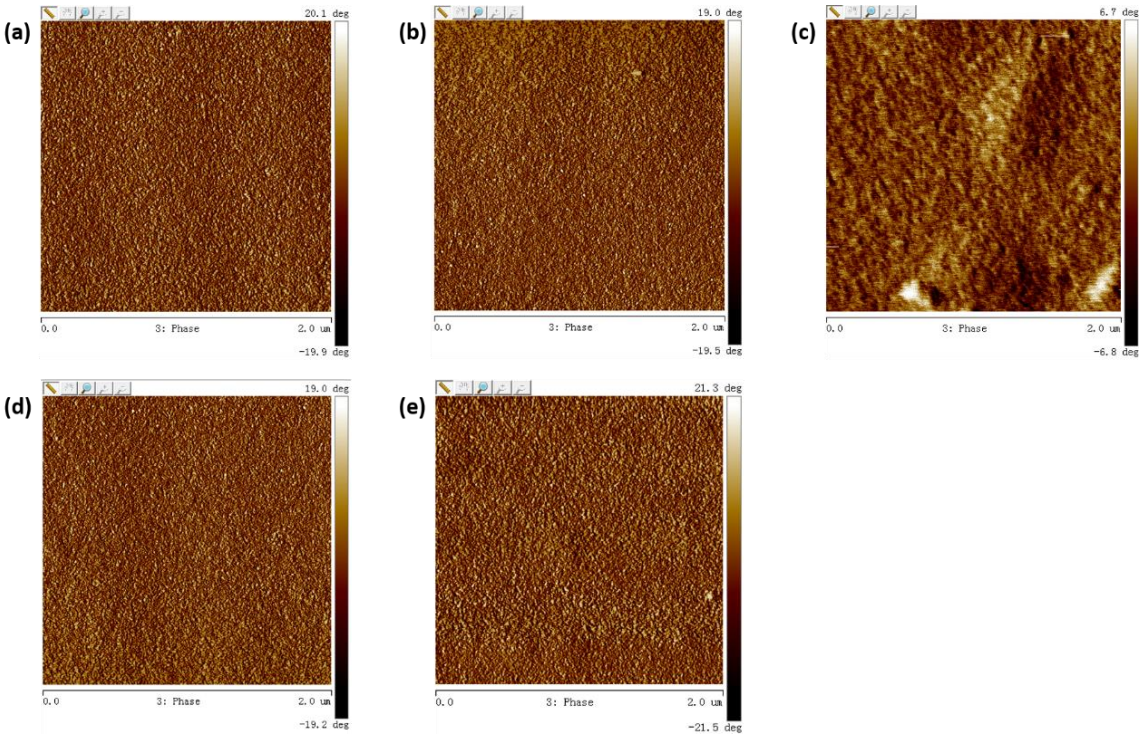

Figure 2.6 Stressing test of SY-PPV:ETPTA:PEO:LiTf (a) luminance vs. time, (b) efficiency vs. time.

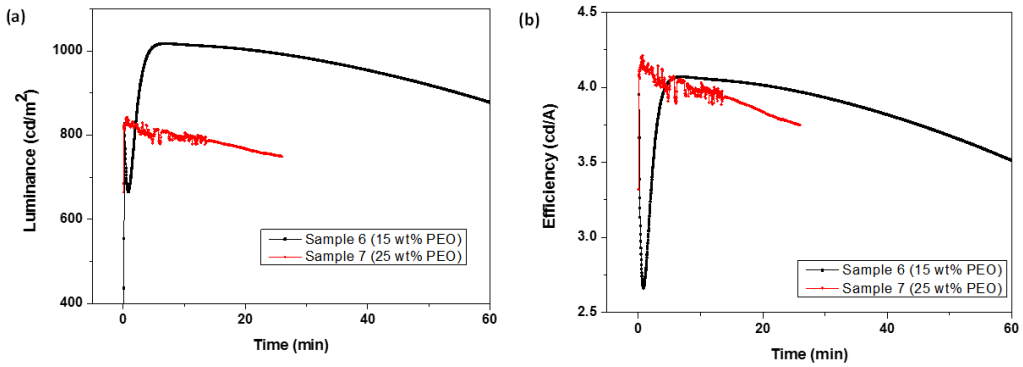

Figure 2.7 AFM phase morphology of (a) sample6, and (b) sample 7.

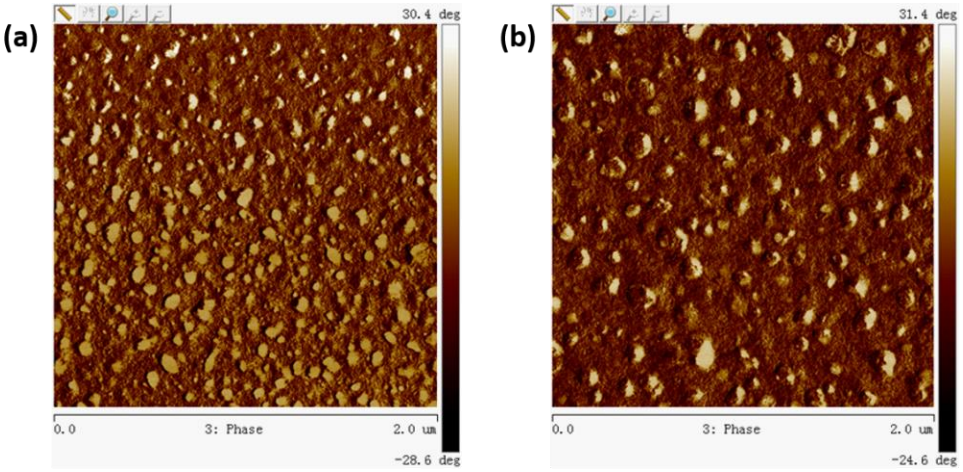

Table 2.1 Weight ratio of different PLEC recipes.

| Sample Name | SY-PPV | ETPTA | LiTf | PEO |
|---|---|---|---|---|
| Sample 1 | 100 | 10 | 1 | |
| Sample 2 | 100 | 10 | 4 | |
| Sample 3 | 100 | 10 | 10 | |
| Sample 4 | 100 | 15 | 4 | |
| Sample 5 | 100 | 20 | 4 | |
| Sample 6 | 100 | 15 | 4 | 15 |
| Sample 7 | 100 | 15 | 4 | 25 |

Table 2.2 Device performance of PLECs with a configuration of ITO/SY-PPV:ETPTA:LiTf/Al under a 3 mA constant current source and 10V compliance.

| | Turn-on Time (min) | Max current density (cd/A) | Max power efficiency (lm/W) | Peak luminance ($cd/m^2$) |
|---|---|---|---|---|
| Sample 1 | 1.5 | 4.38 | 4.73 | 365 |
| Sample 2 | 13.47 | 2.73 | 1.62 | 682 |
| Sample 3 | 9.78 | 2.66 | 1,04 | 666 |
| Sample 4 | 32.8 | 5.96 | 2.88 | 1491 |
| Sample 5 | 0.90 | 4.44 | 2.35 | 1111 |

## 2.6 References


1. Pei, Q.; Yu, G.; Zhang, C.; Yang, Y.; Heeger, A. J. Polymer Light-Emitting Electrochemical-Cells Science 1995, 269, 1086-1088.
2. Pei, Q.; Yang, Y.; Yu, G.; Zhang, C.; Heeger, A. J. Polymer light-emitting electrochemical cells: In situ formation of a light-emitting p-n junction J. Am. Chem. Soc. 1996, 118, 3922-3929.
3. Matyba, P.; Maturova, K.; Kemerink, M.; Robinson, N. D.; Edman, L. The dynamic organic p-n junction Nat. Mater. 2009, 8, 672-676.
4. Pei, Q. B.; Yang, Y. Efficient photoluminescence and electroluminescence from a soluble polyfluorene J. Am. Chem. Soc. 1996, 118, 7416-7417.
5. Shao, Y.; Bazan, G. C.; Heeger, A. J. Long-lifetime polymer light-emitting electrochemical cells Adv. Mater. 2007, 19, 365-370.
6. Fang, J.; Matyba, P.; Edman, L. The Design and Realization of Flexible, Long-Lived Light-Emitting Electrochemical Cells Adv. Funct. Mater. 2009, 19, 2671-2676.
7. Yang, Y.; Pei, Q., Efficient blue-green and white light-emitting electrochemical cells based on poly[9,9-bis(3,6-dioxaheptyl)-fluorene-2,7-diyl] J. of Appl. Phys. 1997, 81, 3294-3298.
8. Yan, H.; Scott, B. J.; Huang, Q.; Marks, T. J. Enhanced polymer light-emitting diode performance using a crosslinked-network electron-blocking interlayer Adv. Mater. 2004, 16, 1948-1953.
9. Zhang, Y.; Gao, J. Lifetime study of polymer light-emitting electrochemical cells J. of Appl. Phys. 2006, 100.
10. Fang, J.; Matyba, P.; Robinson, N. D.; Edman, L. Identifying and alleviating

electrochemical side-reactions in light-emitting electrochemical cells J. Am. Chem. Soc. 2008, 130, 4562-4568.

11. Fang, J. F.; Yang, Y. L.; Edman, L. Understanding the operation of light-emitting electrochemical cells Appl. Phys. Lett. 2008, 9, 063503.
12. Shin, J. H.; Robinson, N. D.; Xiao, S.; Edman, L. Polymer light-emitting electrochemical cells: Doping concentration, emission-zone position, and turn-on time Adv. Funct. Mater. 2007, 17, 1807-1813.
13. Hu, Y.; Tracy, C.; Gao, J. High-resolution imaging of electrochemical doping and dedoping processes in luminescent conjugated polymers Appl. Phys. Lett. 2006, 88, 123507.
14. Wagberg, T.; Hania, P. R.; Robinson, N. D.; Shin, J. H.; Matyba, P.; Edman, L. On the limited operational lifetime of light-emitting electrochemical cells Adv. Mater. 2008, 20, 1744-1749.
15. Robinson, N. D.; Shin, J. H.; Berggren, M.; Edman, L. Doping front propagation in light-emitting electrochemical cells Phys. Rev. B 2006, 74, 155210.
16. Shin, J. H.; Xiao, S.; Edman, L. Polymer light-emitting electrochemical cells: The formation and effects of doping-induced micro shorts Adv. Funct. Mater. 2006, 16, 949-956.
17. Kervella, Y.; Armand, M.; Stephan, O. Organic light-emitting electrochemical cells based on polyfluorene-investigation of the failure modes J. Electrochem. Soc. 2001, 148, H155-H160.
18. Shao, Y.; Gong, X.; Heeger, A. J.; Liu, M.; Jen, A. K. Y. Long-lifetime polymer light-emitting electrochemical cells fabricated with crosslinked hole-transport layers Adv. Mater.

2009, 21, 1972-1975.

19. Yan, H.; Huang, Q.; Scott, B. J.; Marks, T. J. A polymer blend approach to fabricating the hole transport layer for polymer light-emitting diodes Appl. Phys. Lett. 2004, 84, 3873-3875.
20. Gao, J.; Yu, G.; Heeger, A. J. Polymer light-emitting electrochemical cells with frozen p-i-n junction Appl. Phys. Lett. 1997, 71, 1293-1295.
21. Leger, J. M.; Rodovsky, D. B.; Bartholomew, G. R. Self-assembled, chemically fixed homojunctions in semiconducting polymers Adv. Mater. 2006, 18, 3130-3134.
22. Yu, Z. B.; Sun, M. L.; Pei, Q. B. Electrochemical formation of stable p-i-n junction in conjugated polymer thin films J. Phys. Chem. B 2009, 113, 8481-8486.
23. Shin, J. H.; Xiao, S.; Fransson, A.; Edman, L. Polymer light-emitting electrochemical cells: Frozen-junction operation of an "ionic liquid" device Appl. Phys. Lett. 2005, 87, 043506.
24. Yang, C.; Sun, Q.; Qiao, J.; Li, Y. Ionic liquid doped polymer light-emitting electrochemical cells J. Phys. Chem. B 2003, 107, 12981-12988.
25. Becker, H.; Spreitzer, H.; Dreuder, W.; Kluge, E.; Schenk, H.; Praker, I.; Cao, Y. Soluble PPVs with enhanced performance-a mechanic approach Adv. Mater. 2000, 12, 42-48.
26. Spreitzer, H.; Becker, H.; Kluge, E.; Kreuder, W.; Schenk, H.; Demandt, R.; Schoo, H. Soluble phenyl-substituted PPVs-new materials for highly efficient polymer LEDs Adv. Mater. 1998, 10, 1340-1343.
27. Matyba, P.; Yamaguchi, H.; Eda, G.; Chhowalla, M.; Edman, L.; Robinson, N. D. Graphene and mobile ions: the key to all-plastic, solution-processed light emitting devices ACS Nano 2010, 4, 637-642.

28. Yu, Z.; Wang, M.; Lei, G.; Liu, J.; Li, L.; Pei, Q. Stabilizing the dynamic p-i-n junction in polymer light emitting electrochemical cells J. Phys. Chem. Lett. 2011, 2, 367 -372.

29. Malliaras, G.; Friend, R. An organic electronics primer Physics Today 2005, 58, 53-58.

30. Yin, K.; Zhang, L.; Lai, C.; Zhong, L.; Smith, S.; Fong, H.; Zhu, Z. Photoluminescence anisotropy of uni-axially aligned electrospun conjugated polymer nanofibers of MEH-PPV and P3HT J. Mater. Chem. 2011, 21, 444-448.

31. Sandström, A.; Matyba, P.; Edman, L. Yellow-green light-emitting electrochemical cells with long lifetime and high efficiency *Appl. Phys. Lett.* 2010, 96, 053303.

32. Hu Y.; Gao, J. Cationic effects in polymer light-emitting electrochemical cells *Appl. Phys. Lett.* 2006, 89, 253514.

33. Van Reenen, S.; Matyba, P.; Dzwilewski, A.; Janssen, R.A.J.; Edman, L.; Kemerink, M. Salt concentration effects in Planar Light-Emitting Electrochemical Cells Adv. Funct. Mater. 2011, 21, 1795-1802.

34. Parker, I. D.; Cao, Y.; Yang, C. Y. Lifetime and Degradation Effects in Polymer Light-Emitting Diodes J. Appl. Phys. 1999, 85, 2441-2447.

35. Li, Y.; Gao, J.; Wang, D.; Yu, G.; Cao, Y.; Heeger, A. J. A.C. impedance of frozen junction polymer light-emitting electrochemical cells Synth. Met. 1998, 97,191-194.

36. Bard, A. J.; Faulkner, L. R. Electrochemical methods: fundamentals and applications (2nd edition) 2000.

37. Pei, Q.; Heeger, A. J. Operating mechanism of light-emitting electrochemical cells Nat. Mater. 2008, 7, 167-168.

38. Tang, S.; Irgum, K.; Edman, L. Chemical stabilization of doping in conjugated polymers

Org. Electron. 2010, 11, 1079–1087.

39. Habrard, F.; Ouisse, T.; Stephan, O.; Aubouy, L.; Gerbier, P.; Hirsch, L.; Huby, N.; Van der Lee, A. Organic light-emitting diodes and organic light-emitting electrochemical cells based on silole-fluorene derivatives Synth. Met. 2006, 156, 1262-1270.
40. Shoji, T. D.; Zhu, Z.; Leger, J.M. Characterizing ion profiles in dynamic junction light-emitting electrochemical cells ACS Appl. Mater. Interfaces 2013, 5, 11509-11514.
41. Edman, L. Bringing light to solid-state electrolytes: the polymer light-emitting electrochemical cell Electrochem. Acta. 2005, 50, 3878-3885.

# Chapter 3 Elastomeric light emitting polymer enhanced by interpenetrating networks

## 3.1 Introduction

Deformable electronic devices have attracted increasing attention in recent years thanks to the emerging interests in wearable electronics and biomedical applications. Stretchable devices made by embedding rigid active electronic components in a soft rubbery polymer substrate, employing buckled interconnects, and ultrathin films on pre-strained substrates have been explored [1-16]. Electronic skins [17-19], wearable electronics [20,21], and flexible displays [22,23] have been fabricated to demonstrate the breadth and enthusiasm for the stretchable devices. Progress has also been reported on stretchable polymer light emitting devices [24-27]. However, intrinsical large-strain stretchability in which the entire device can be deformed like an elastomer, i.e., the deformation is both globally and locally uniform [28,29], remains a fundamental challenge as the electronic materials should be stretchable. We reported stretchable transparent conductors based on a percolation network of silver nanowires (AgNWs) or carbon nanotubes embedded in the surface of an elastomer substrate [24,26]. AgNWs have been more and more popular because of the promising electrical property comparable to that of well know indium tin oxide (ITO), and optical transparency [22, 30-32]. Stretchable polymer light emitting electrochemical cells (PLECs) have also been reported in which a blend film consisting of a conjugated polymer and ionically conductive solid electrolyte was laminated between a pair of stretchable transparent electrodes [25]. The PLEC could be stretched by as much as 120%. While significant degradation was observed at such extreme deformation, the deformation at small strains, such as 30%, was largely elastic. The conjugated polymer, a

soluble alkyloxy phenyl substituted poly(1,4-phenylene vinylene) (SY-PPV) with bright yellow fluorescent emission is known to lack such elastomeric deformability. Little is known or has been investigated on how the polymer blend could withstand large-strain stretching. A fundamental understanding may lead to a general approach to imparting rubbery elasticity to conjugated polymers that are otherwise unstretchable.

Stretchable polymer light emitting diodes (PLEDs) wherein a neat conjugated polymer was employed as the emissive layer were also demonstrated. Deformable charge injection layers have to be employed in the PLEDs, and the deformability of these layers, as well as interfacial bonding, all complicates the stretchability of the emissive layer. The PLEC features a much simpler device structure, and thus provides an ideal platform to investigate the mechanical deformation of the semiconductor layer. A typical PLEC device has an electroluminescent layer sandwiched between two electrodes [33]. The electroluminescence layer is an ionic and electronic mixed conductor system wherein the conjugated polymer provides the electronic networks while an ionic conductive medium furnishes cations for n-doping and anions for p-doping of the conjugated polymer at the cathode and anode, respectively. The in-situ formation of a P-I-N junction in the polymer blend layer facilitates electron and hole injection from the cathode and anode respectively, and thus AgNWs could be used for both electrodes. Here, the morphology of the electronic and ionic mixed conductors on a polyurethane elastomer substrate has been investigated in connection with elastomeric deformability. The morphology reveals an interpenetrating polymer network (IPN) structure with the electronic conductor, SY-PPV, forms a continuous network, and the ionic phase fills the pores. This microstructure, somewhat analogous to water soaked sponge, can be repeatedly

stretched at 50% strain for at least 1000 cycles. No plastic deformation or chain re-orientation of SY-PPV was observed during stretching, which would have induced a large dichroic ratio in optical absorption [34] and photoluminescence [35]. PLECs fabricated by laminating this mixed conductor layer between two AgNW-based transparent composite electrodes could survive a linear strain up to 140%. No polarization of the electroluminescence intensity was observed.

A few parameters can be used to quantify materials resistance to failure, which in turn defines the usefulness of a polymer under a certain applied condition. The failure under a harsh/rigorous condition which requires a stronger external stress and absorbing more energy would be preferential. Understanding morphological geometry, processing history, and test condition would be a guidance for materials selection and optimization under different mechanical loading modes. Polymers are possible to be toughened by incorporating a plasticizer into the polymer.

### 3.2 Experimental methods

***Materials.*** Soluble Super Yellow (SY-PPV, phenyl substituted poly(1,4-phenylene vinylene), molecular weight: $1.94X10^6$ g/mol) was obtained from Merck (catalog #: PDY-132). Silver nanowire (AgNW) was purchased from Zhejiang Kechuang Adv. Mater. Tech Co. Ltd (average diameter: 25-35nm; average length: 10-20μm). Lithium trifluoromethane sulfonate (LiTf, 99.995% purity), poly (ethylene oxide) (PEO, $T_g \approx 267℃$; $M_v \approx 100{,}000$, where $M_v$ is the average molecular weight determined by viscosity), polyethylenimine (PEI) in methoxyethanol (diluted by adding 2-methoxyethanol to 0.4wt%), 2,2-dimethoxy-2-phenylacetophenone (99%,

DMPA) and anhydrous tetrahydrofuran (THF) were obtained from Sigma-Aldrich. ETPTA (SR9035), CN990, and SR541 were supplied by Sartomer. Poly(3,4-ethylenedioxythiophene):poly(styrenesulfonate) (PEDOT:PSS) was obtained from H.C. Starck (Clevios VP PH1000). 2-methoxyethanol (99%) was bought from Acros. A thermally crosslinkable urethane liquid rubber compound (ClearFlex95, mixed at a weight ratio of 2:3 parts A:B) was obtained from Smooth-On USA and used as transparent elastic substrate. All materials were used as received.

***Sample preparation.*** Glass slides were cleaned by acetone and isopropanol (IPA). A solution of SY-PPV, PEO, ETPTA, and LiTf in THF (weight ratio 100:15:15:4; 4mg/mL of SY-PPV) was spin-coated at 900 rpm for 60s onto the glass slide. The film was then dried at 70℃ for 30min to remove residue THF. The resulting electroluminescence polymer layer on the glass was then coated with a pair of pre-crosslinked ClearFlex 95 layer at 110 ℃ for 10min and peeled off as a free-standing film. A polarizer film was placed between the sample and photoluminescence detector so that only light from selected direction was collected.

***Light emitting device sample preparation.*** A dispersion of AgNWs (~2 mg/mL) was diluted in IPA and coated onto a glass substrate with a Meyer rod. A precursor solution consisting of CN990 (siliconized urethane acrylate oligomer), SR541 (ethoxylated bisphenol A dimethacrylate) and DMPA (photoinitiator) (weight ratio 100:20:0.5) was coated onto the AgNW-glass substrate and cured through a Dymax ultraviolet conveyor equipped with 2.5W/cm$^2$ Fusion 300S type ‘H’ ultraviolet curing bulb, at a speed of 1.0feet per min for one pass before peeling off as a free-standing AgNW-PUA electrode substrate A sheet resistance of 20Ω/□ AgNW-PUA composite electrode was then cleaned by detergent followed by

deionized water and IPA. PEDOT:PSS was then spin-coated on the composite electrode at 4500 rpm for 60s, followed by 20min 70℃ anneal and 30min vacuum evaporation to remove residual water. This PEDOT:PSS coated AgNW-PUA composite electrode was used as anode. AgNW-PUA composite electrode spin-coated with PEI at 5000 rpm for 60s and dried in vacuum was also prepared as cathode. The cathode was laminated, with the conductive layer facing down onto the active polymer layer and heated to 90 ℃ to enhance adhesion between the layers. The stack was then hot pressed at 270 ℃. And thus the polymer light emitting electrochemical cell (PLEC) device had a thin film sandwich structure of AgNW-PUA/PEDOT:PSS/multi-ingredient blend film(SY-PPV, PEO, ETPTA and LiTf at weight ratio 100:15:15:4, 7mg/ml of SY-PPV)/AgNW-PUA, and the polymer light emitting diode (PLED)device is composed of AgNW-PUA/PEDOT:PSS/SY-PPV (7mg/mL)/PEI/AgNW-PUA. The thickness of the luminescent active layer was ~180 nm.

***Characterization.*** UV-vis absorbance spectra were collected by Shimadzu UV-1700 spectrophotometer. Photoluminescence (PL) spectra were recorded by Photon Technology International spectrophotometer. Scanning electron microscope (SEM) was imaged on a JEOL JSM-6710F scanning electron microscope. AFM measurements were carried out in PeakForce QNM (Quantitative NanoMechanics) mode on a Bruker dimension icon scanning probe microscope at ambient conditions. A commercial silicon cantilever (RTESPA-150) was used in this study. RTESPA-150 has a typical radius of curvature of ~8 nm and a nominal spring constant of ~5 N/m. NanoMechanical mapping was operated at constant peak force. Light emitting test was carried out in a glove box, with oxygen and moisture levels below 0.5 ppm. The current density -luminance-voltage curves for stretchable PLEC and PLED in their pristine

state (0% strain) were recorded with a Keithley 2400 source meter and a calibrated silicon photo-detector by sweeping applied voltage from 0 to 21V in 200mV incremental steps. The luminance data and electroluminescent spectrum for PLEC and PLED under stretched states were measured with a Photoresearch PR-655.

### 3.3 Results and discussions

#### 3.3.1 Interpenetrating network formation.

SY-PPV was selected as the organic semiconductor material due to its high molecular weight ($1.94*10^6$ g/mol), solubility in common organic solvents, high photoluminescence (PL) and electroluminescence (EL) quantum yields [36-41]. The delocalization of $\pi$-electrons along the poly(1,4-phenylene vinylene) main chain makes SY-PPV rigid with high stiffness, despite the presence of long-chain alkyl side groups [42]. Admixing with a soft additive could ease the deformation of SY-PPV, in a similar fashion as polymers are plasticized. However, not all morphologies are desirable, as in semiconductor devices the SY-PPV must form a continuous phase to carry electrons and holes from one electrode to the other. Poly (ethylene oxide) (PEO) was chosen as the soft medium thanks to its low glass transition temperature and its wide use in solid electrolyte as an ionic conductor [33]. A PEO with modestly long chain length (Mv~100,000) was used such that the blend with SY-PPV is not too viscous. An exoxylated trimethylolpropanetriacrylate (ETPTA) was added into the blend to 1) improve the elasticity as cured ETPTA forms a highly crosslinked network and 2) enhance the miscibility between SY-PPV and PEO as ETPTA contains both oligo(ethylene oxide) moiety and hydrocarbon moiety. ETPTA was also found to help stabilize the P-I-N junction in the operation of PLEC

devices [24, 37, 38]. Lithium trifluoromethanesulfonate (LiTf) was added into the blend as the source for ions. The weight ratio of the multi-ingredient blend SY-PPV:PEO:ETPTA:LiTf used here was 100:15:15:4, selected after dubious experimental examinations of the trade-off between stretchability and electroluminescence. Further increasing the amount of PEO and ETPTA in the blend induced more severe phase separation from SY-PPV and worse electroluminescent behavior. Tetrahydrofuran (THF) has a low boiling point of 66 $^{o}$C; its rapid vaporization during spin coating tends to produce amorphous and randomly oriented polymer chains in the film. The above ingredients were co-dissolved in THF. The resulting solutions were spin-casted to form thin films.

Scanning electron microscope (SEM) image in Figure 3.1a shows that the spin-cast, multi-ingredient blend film has phase separated morphology. The resolution or contrast is not sufficiently high, and does not give much information on which component is dominant in each phase. Atomic force microscope (AFM), as an alternative method to gather information on surface morphology and phase separation, has been used to characterize soft materials [43] where small force and small deformation is required for topography. PeakForce Quantitative NanoMechanical (QNM) mapping is a specific AFM imaging method that records force curves pixel by pixel and integrates them into surface quantitative mechanical properties map [44, 45]. Local elastic moduli could be derived from the unloading portion of the force vs. deformation curves using Derjauin-Muller-Toporov (DMT) model [46]. The AFM probe tip is approximately spherical at the very end, with a tip radius of ~8nm, which fits well with DMT model.

Here, we used PeakForce QNM mapping mode at ambient condition to examine neat SY-PPV, solid electrolyte (PEO:ETPTA:LiTf), and the multi-ingredient PLEC blend (SY-PPV:PEO:ETPTA:LiTf) samples to obtain their surface morphology and the distribution of Young's modulus (Figure 3.1b-3.1f). Figure 3.1b is QNM mapping image of a neat SY-PPV film with an average modulus of 201±4MPa. Continuously and smoothly distributed surface modulus mapping feature can be found in the neat SY-PPV sample. Similarly uniform modulus distribution is observed for the solid electrolyte (Figure 3.1c), though the average modulus is lowered by one-half, 100±2MPa. Young's modulus mapping of the PLEC blend composite sample (Figure 3.1d) reveals major phase separations, with the continuous phase (lighter color) having a modulus value of 178±7MPa, while the isolated islands (deeper color) are much softer with a modulus value of 72±5MPa. The modulus of the continuous phase is not far from the value of the neat SY-PPV. Since SY-PPV is also the majority part in the PLEC blend film, this continuous phase should be dominated by SY-PPV, which has low polarity. The polar or ionic ingredients, PEO, ETPTA and LiTf together forms the isolated island phase with a much lower modulus. The moduli of the two separated phases are slightly lower than the respective neat SY-PPV and solid electrolyte. We speculate that in the continuous SY-PPV phase, there is a small amount of the polar and ionic ingredients, perhaps more likely ETPTA which is bipolar is dissolved in the SY-PPV phase and slightly plasticizes the conjugated polymer matrix. The lower modulus of the electrolyte phase in the blend could be caused by its viscoelasticity which exhibits a lower modulus than the neat solid electrolyte in smaller dimensions. Another reason that the modulus decreases in the electrolyte phase might be the

nonlinearity of the stress-strain relationship in small indentations [42]. The solid electrolyte phase is ~100nm in diameter on average.

When the PLEC blend is stretched by 50% strain, the QNM image shows that the Young's modulus in the continuous phase is slightly increased to 182±10MPa, while the solid electrolyte phase is increased to 77±10MPa. Figure 3.1f plots the Young's modulus profiles of all the samples. The large variations of modulus for the PLEC blend are in stark contrast to the neat SY-PPV and solid electrolyte samples. The solid electrolyte phase reveals oval shapes under 50% strain along the stretching direction, with the long axis length ranging from 120nm to 160nm. SEM images in Figure 3.2 also featured such oval shapes along the stretching direction. There are no wrinkles or cracks observable. However, Figure 3.2b of the neat SY-PPV film under 50% strain shows vertical crack lines.

### 3.3.2 Dichroism of optical absorption

UV-vis absorption spectra were taken to study the influence of strain on the polarization of the neat SY-PPV and multi-ingredient PLEC blend (SY-PPV, PEO, ETPTA, and LiTf). The polarization properties were measured by rotating a polarizer placed between the sample and detector to probe light intensity along the polarizer direction. The sampling area was 12.56 $mm^2$ for all the samples. The parallel direction (marked as "//") is defined as the polarizer in parallel to the stretching direction; the perpendicular direction (marked as "⊥") is when the polarizer is orthogonal to stretching direction.

Figure 3.3 and Figure 3.4 show the UV-vis absorbance spectra at different stages during stretching and relaxation. The absorbance peak of the neat SY-PPV and multi-ingredient PLEC

blend is at 440nm in fresh films (0% strain). In each sample, the shape of the absorbance spectrum in parallel and perpendicular directions coincide with each other, indicating no preferential alignment in random SY-PPV chains. Dichroic ratio (DR), defined in equation (1), indicates the alignment of conjugated polymer (SY-PPV in this case) backbone along the direction of strain.

$$\mathrm{DR} = \frac{Abs_{//}}{Abs_{\perp}} \qquad (1)$$

Where $Abs_{//}$ and $Abs_{\perp}$ are the absorbance value at parallel and perpendicular direction. DR is calculated using the maximum absorbance value in the spectra and listed in Table 3.1.

For neat SY-PPV samples, the absorbance dichroism becomes more significant when the strain is larger than 30%. DR value increases from 1.00 to 2.32 when strain was increased from 0 to 100%. The increasing dichroism (DR values) is in agreement with the widely reported molecular alignment of stretched conjugated polymers along the elongated axis [47-49]. To further investigate the impact of strain on the absorption differentiation at the orthogonal directions, samples relaxed from applied strain were also studied. A sample under certain strain was released and left for 30 min to allow fully relaxation before UV-abs measurement again. DR values range from 1.12 to 1.41, indicating that the alignment of SY-PPV molecular is irreversible. All SY-PPV samples showed higher absorbance intensity in direction parallel to which strain was once applied. The intensity of absorbance peak at the parallel direction is higher than that of the fresh film, which is possibly originated from the formation of nanosized buckles at the surface of SY-PPV film leading to an increased light path in the corrugated structure [50].

In the multi-ingredient PLEC blend sample, peak intensity at orthogonal directions is quite identical at each specific strain or relaxation from certain strain. DR values are almost equal to 1.00, indicating no preferential oriented direction, thus no polarization in the PLEC blend film.

### 3.3.3 Dichroism of photoluminescence

PL anisotropy measurement was carried out using 450nm excitation wavelength from an argon laser source and spectra are presented in Figure 3.5 and Figure 3.6. The fluorescence dichroic ratio $R_{ex}$ is defined [51] in equation (2).

$$R_{ex} = \frac{I_{//}}{I_{\perp}} \qquad (2)$$

Where $I_{//}$ and $I_{\perp}$ are the fluorescence intensity measured at parallel and perpendicular direction. $R_{ex}$ is calculated at maximum emission of the irradiated film and summarized in Table 3.2.

Figure 3.5 and Figure 3.6 show the PL emission spectra at different stages during stretching and relaxation. The trend observed from PL data is in consonance with UV-vis absorbance results. For the neat SY-PPV sample, $R_{ex}$ ranges from 1.00 to 2.09 when being stretched from 0% to 100%; and 1.55 to 2.07 after strain was released. The emission under polarized light was enhanced in the stretching direction. $R_{ex}$ is ~1.00, fluctuating in a fairly narrow range of ±3%, at each strain level for PLEC sample.

The absorbance and PL spectra show evidence that SY-PPV film is plastically deformed. The amorphous SY-PPV chains are aligned along strain direction, and dichroism is enhanced with increasing strain. However, admixing ionic solid electrolyte (PEO and ETPTA) into SY-PPV helps to suppress the anisotropic polarization behavior under strain. The multi-ingredient

PLEC sample deforms elastically in response to external strain. It is likely that the deformation of the PLEC blend morphologically causes the porous solid electrolyte to align along strain direction. The continuous SY-PPV mesh in the blend largely retains the randomness of SY-PPV chains. As a result, the non-oriented SY-PPV chains give isotropic absorption and emission spectra in the orthogonal directions. A schematic overview of such phase morphology in response to strain is represented in Figure 3.7.

### 3.3.4 Stretchable PLEDs and PLECs

Light emitting devices were also made to investigate light emitting polarization behavior under strain. Stretchable PLEC and PLED were fabricated on a fully stretchable elastomeric silver nanowire-polyurethane (AgNW-PUA) substrate, where all components were elongated at the same pace when being stretched. Poly(3,4-ethylenedioxythiophene):poly(styrenesulfonate) (PEDOT:PSS) was used as hole transporting layer while polyethylenimine (PEI) functioned as the electron transporting layer to enhance electron injection into PLED device. PLEC device has an architecture of AgNW-PUA/PEDOT:PSS/PLEC blend (100:15:15:4 of SY-PPV:PEO:ETPTA:LiTf, by weight)/AgNW-PUA. PLED device has a thin film sandwich structure of AgNW-PUA/PEDOT: PSS/SY-PPV/PEI/AgNW-PUA. Both PLEC and PLED were made from solution-based coating and lamination process. Device performance under strain was studied at room temperature in a dry nitrogen filled glovebox. The current density-luminance-driving voltage response (J-L-V) is shown in Figure 3.8a and b. Polarized light emitting luminescence

(Figure 3.8e and f) were measured by PR655, with a polarizer film placed in front of the lens to select polarization direction.

A typical PLEC device J-L-V curve is presented in Figure 3.8a. Light emission in this PLEC turns on at 3 V and reaches a peak brightness of 1750 cd/m$^2$ at 19 V. Figure 3.8b is the PLED J-L-V curve. The electroluminescence turns on at around 13V and reaches a brightness of 325 cd/m$^2$ at 20 V. PLEC device can be uniaxially stretched up to 140% before luminance fell to 10% of the value when device was initially driven. Figure 3.5c shows the luminance data vs. increasing strain rate when PLEC device was biased at 12V. All the luminance values presented in Figure 3.8c were from the central area of the light emitting region (an area that is quite representative and can be compared among different samples). The brightness fluctuates in the strain range of 40%-100%. The cause for this irregular trending of the luminance is not clear. One possibility is that the film flatness varies slightly with strain. Some crack formation was observed in the PEDOT:PSS layer upon large strain [25]. But such crack formation only affects a small fraction of the interfacial areas and does not significantly alter the operation of the PLEC device. Figure 3.5d is the EL spectra of PLEC device captured at different strains. The wavelength at the peak of each EL spectrum and the shape of the curve at each strain rate does not change. The difference lies in the value of peak radiance, which is an alternative way to describe luminescence. 50% strain was used here to investigate the influence of strain on light emitting polarization due to its moderate luminescence and lighting stability at such fairly large strain. Table 3.3 is the polarized luminance data of PLEC and SY-PPV PLED device calibrated by PR655. Figure 3.5e and f shows polarized EL spectra at the orthogonal directions relative to stretching direction at 0% and 50% strain. Characterizations of multi-ingredient

PLEC blend samples were carried out after PLEC was initially charged under a constant 12V for 5min to guarantee stabilized P-I-N junction formation. SY-PPV PLED samples were driven under a constant 18V source. In the PLEC device, light intensity in the two directions was almost the same and decreased to half when stretched to 50%. In SY-PPV PLED device, luminance intensity at parallel direction is higher than perpendicular direction by 16% at 0% strain. The luminance reduced to one-third when 50% strain was applied and the difference between the parallel and perpendicular direction was 100% in the PLED device. More than ten devices were tested, with performance (luminance) fluctuating in a fairly reasonable range of ±10%, indicating good reproducibility and reliability. In SY-PPV PLED device where no IPN network exists, light intensity in the direction parallel to the polarizing direction is significantly higher than the perpendicular direction under strain. The minor variation of radiance in different directions could be caused by non-uniformity of the PU substrate, the AgNW network, and/or the interlayers such as PEI, PEDOT:PSS. The PLEC performance exhibits that light in orthogonal directions is nearly the same no matter whether this blended emissive layer is stretched or not. The SY-PPV chains are prevented from being oriented under strain due to the existence of IPN, where the solid electrolytes accommodate deformation energy to keep the continuous mesh phase as a whole. The addition of PEO and ETPTA not only forms IPN network with SY-PPV, but also ensures the isotropic light emitting performance in orthogonal directions.

### 3.4 Summary

In summary, the PLEC blend based on SY-PPV:PEO:ETPTA:LiTf forms an interpenetrating network (IPN), exhibiting rubbery elasticity at room temperature. PeakForce QNM mapping images reveal a detailed insight of the nanoscopic morphology and moduli distribution of the PLEC blends. The PLEC blend is comprised of a porous phase, which can accommodate deformation along strain direction. Such deformation does not induce orientation from SY-PPV polymer chains, and the polymer chains retain randomness at large strains up to 100%. PLEC device could be stretched up to 140% strain before luminescence decreased to 10%. Although the study is not exhaustive, it does point to an IPN morphology wherein a rigid conjugated network, in the form of a mesh, intercalated with soft pockets comprised of the ionically conductive additives is a suitable medium to allow large strain deformation.

### 3.5 Figures

Figure 3.1 (a) SEM top view image of an SY-PPV:PEO:ETPTA:LiTf blend sample (100:15:15:4 by weight percent); DMT modulus mapping of (b) neat SY-PPV film, (c) solid electrolyte (PEO, ETPTA, and LiTf, 15:15:4 by weight), SY-PPV:PEO:ETPTA:LiTf blend (100:15:15:4 by weight) at 0% strain (d) and 50% strain (e); (f) Young's modulus vs. position sectioning curves corresponding to the cross sections of the white dash line in (b-e).

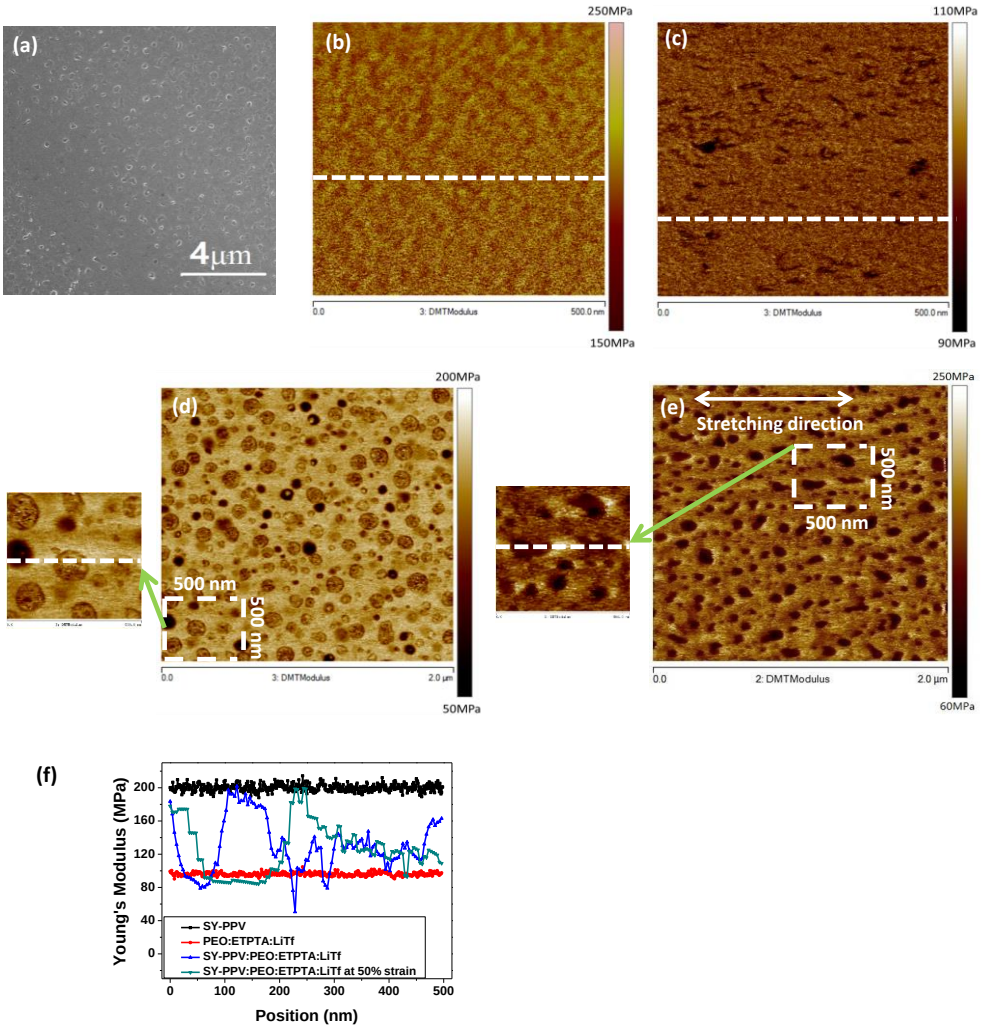

Figure 3.2 SEM images of (a) multi-ingredient blend film (SY-PPV:PEO:ETPTA:LiTf), (b) neat SY-PPV sample under 50% strain after 1000 cycles of repeated stretching-relaxation between 0 and 50% strain.

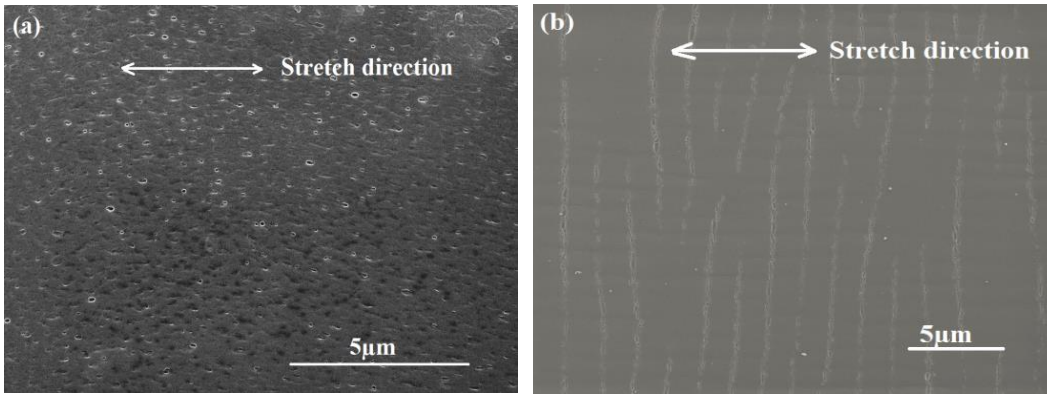

Figure 3.3 UV-vis absorbance spectra of SY-PPV film at different stages during stretching (0, 30, 50, 70 and 100%) or released from certain strain (30, 50, 70 and 100%) as is denoted in the figures.

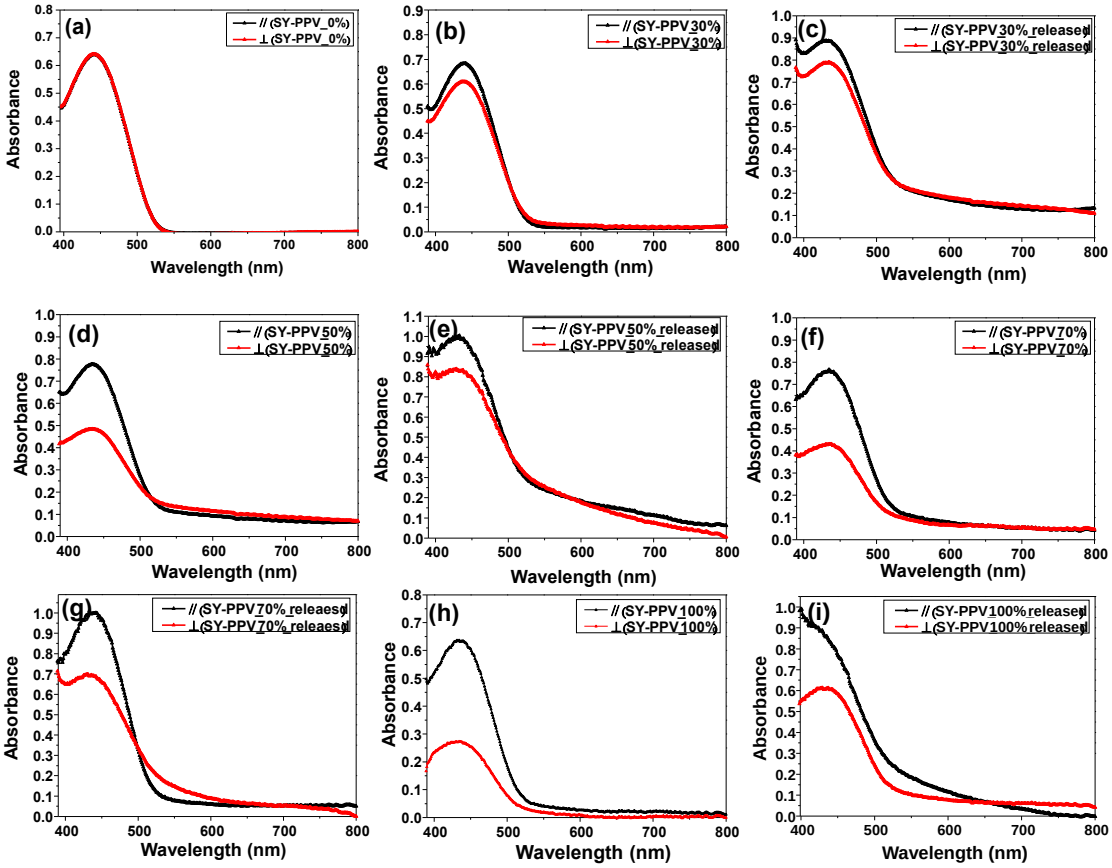

Figure 3.4 UV-vis absorbance spectra of blended film at different stages during stretching (0, 30, 50, 70 and 100%) or released from certain strain (30, 50, 70 and 100%) as is denoted in the figures.

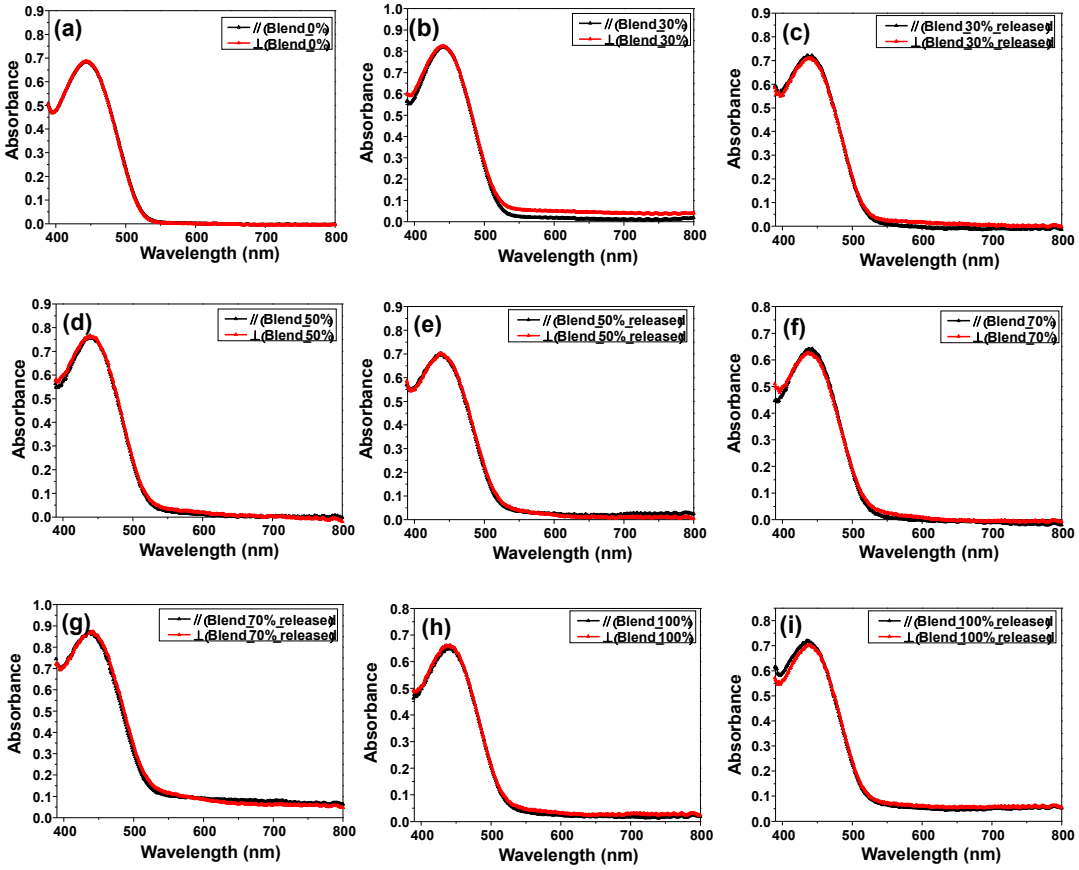

Figure 3.5 Anisotropic fluorescence emission of neat SY-PPV sample at at different stages during stretching (0, 30, 50, 70 and 100%) or released from certain strain (30, 50, 70 and 100%) as is denoted in the figures

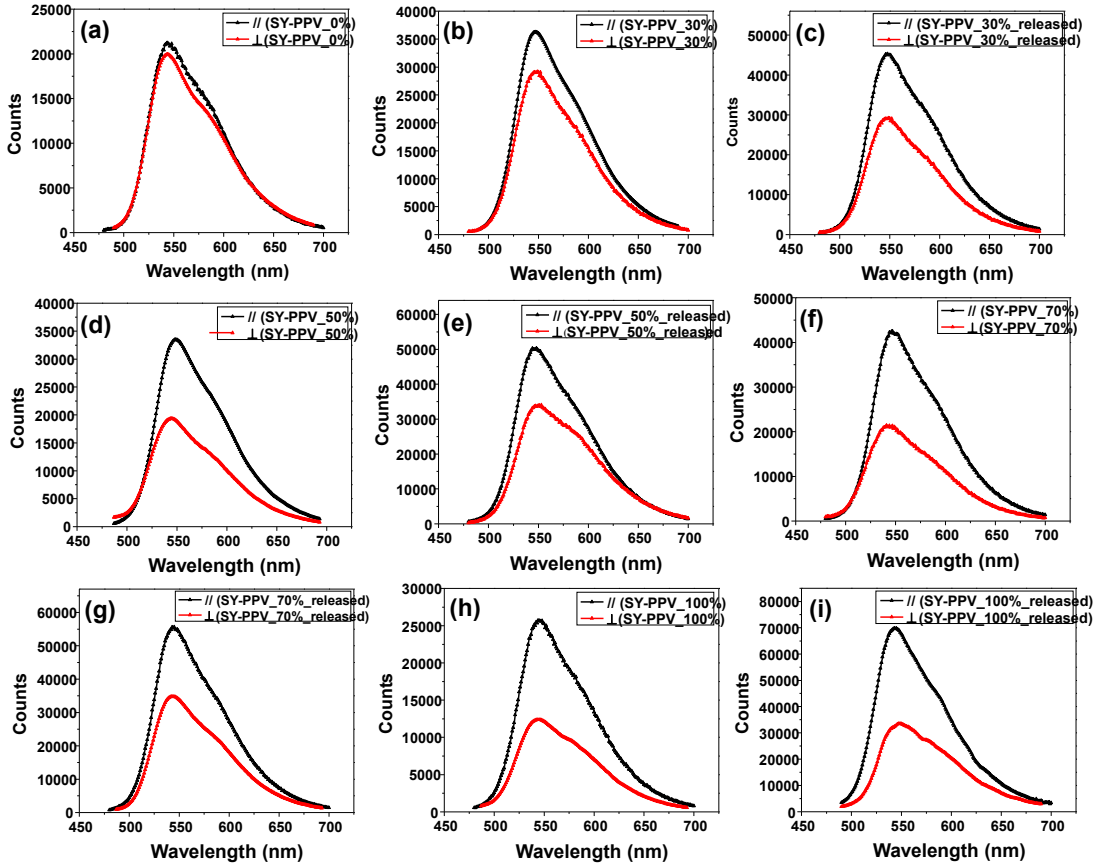

Figure 3.6 Isotropic fluorescence emission of PLEC blend sample at different stages during stretching (0, 30, 50, 70 and 100%) or released from certain strain (30, 50, 70 and 100%) as is denoted in the figures.

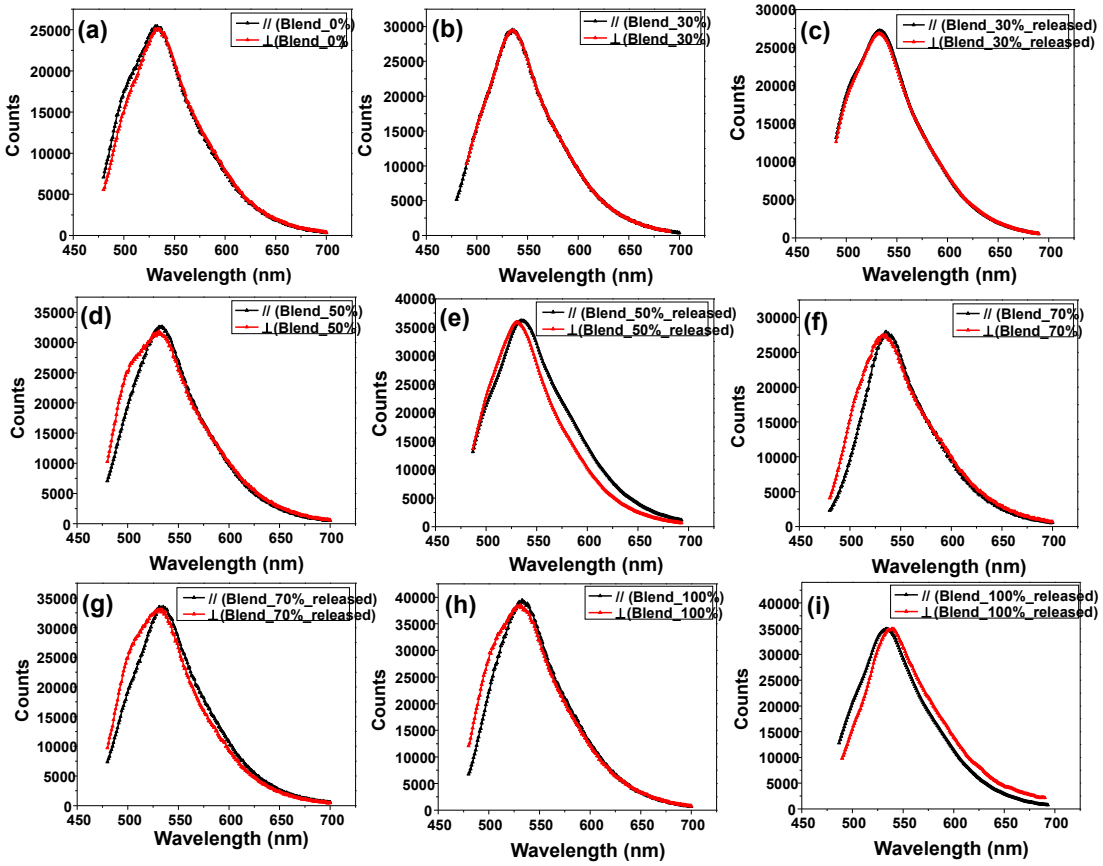

Figure 3.7 Schematic view of the phase morphology of (a) a PLEC blend film in response to uniaxial stretching, and (b) nest SY-PPV in response to uniaxial stretching.

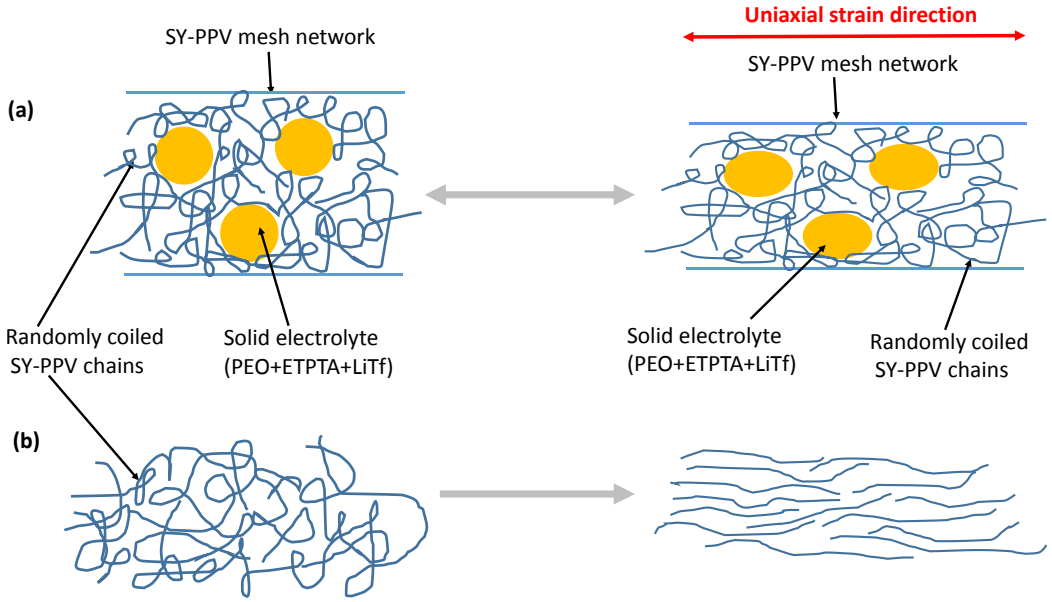

Figure 3.8 Current density and luminance vs. bias (J-L-V) diagrams of (a) PLEC, (b) SY-PPV PLED; (c) Luminance vs. strain of the PLEC; (d) Radiance intensity vs. wavelength spectra at specified strain corresponding to (c); Polarized radiance intensity of (e) PLEC and (f) SY-PPV PLED. "∥" is radiance along the stretching direction and "⊥" the orthogonal direction. Inserted in (c) are optical photographs of PLEC biased at 12V at 0% and 50% strain, respectively.

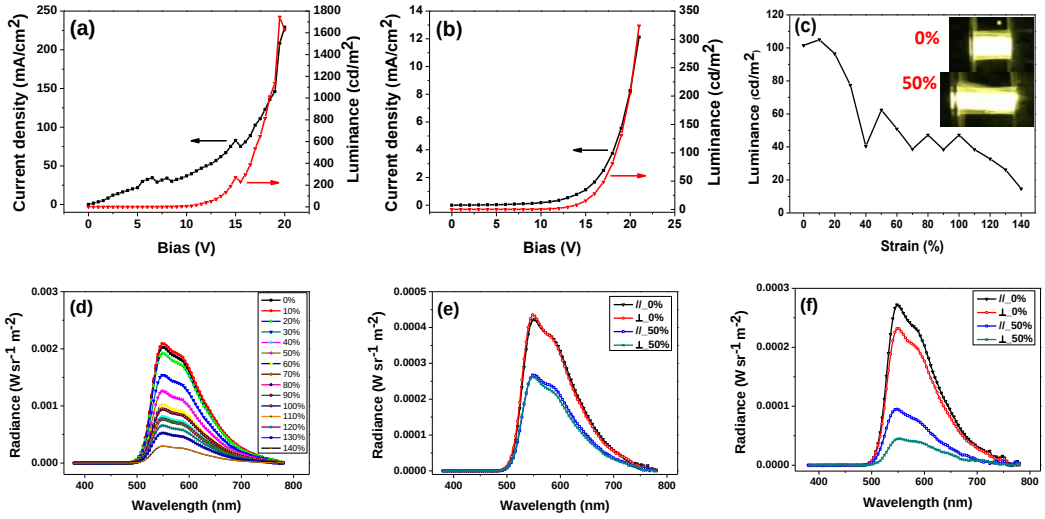

Table 3.1. DR ratio calculated from neat SY-PPV and multi-ingredient blend sample

| Strain | Dichroic Ratio | | | |
|---|---|---|---|---|
| | SY-PPV sample | | PLEC blend sample | |
| | Stretched | Relaxed from strain | Stretched | Relaxed from strain |
| 0% | 1.00 | | 1.00 | |
| 30% | 1.12 | 1.12 | 1.00 | 1.00 |
| 50% | 1.66 | 1.15 | 1.00 | 1.00 |
| 70% | 1.78 | 1.24 | 1.00 | 1.00 |
| 100% | 2.33 | 1.41 | 1.00 | 1.03 |

Table 3.2. $R_{ex}$ calculated from neat SY-PPV and multi-ingredient blend sample

| Strain | Dichroic Ratio | | | |
|---|---|---|---|---|
| | SY-PPV sample | | PLEC blend sample | |
| | Stretched | Relaxed from strain | Stretched | Relaxed from strain |
| 0% | 1.07 | | 1.00 | |
| 30% | 1.25 | 1.55 | 1.00 | 1.01 |
| 50% | 1.73 | 1.54 | 1.02 | 1.01 |
| 70% | 1.99 | 1.59 | 1.01 | 1.01 |
| 100% | 2.09 | 2.07 | 1.03 | 1.00 |

Table 3.3. Luminance data of stretchable PLED and PLEC devices

| Luminance (cd/m2) | 0% Stretching | | 50% Stretching | |
|---|---|---|---|---|
| | parallel | perpendicular | parallel | perpendicular |
| SY-PLED | 13.21 | 11.38 | 4.630 | 2.276 |
| PLEC blend | 21.04 | 21.32 | 13.32 | 12.89 |

### 3.6 References


1. Camposeo, A.; Persano, L.; Pisignano, D. Light-emitting electrospun nanofibers for nanophotonics and optoelectronics Macromol. Mater. Eng. 2013, 298, 487-503.
2. Vosgueritchian, M.; Tok, J.B. H.; Bao, Z. Stretcahble LEDs: light-emitting electronic skin Nat. Photonics 2013, 7, 769-771.
3. Benight, S. J.; Wang, C.; Tok, J. B. H.; Bao, Z. Stretchable and self-healing polymer and devices for electronic skin Prog. Polym. Sci. 2013, 38, 1961-1977.
4. Rogers, J. A.; Someya, T.; Huang, Y. Materials and mechanics for stretchable electronics Science 2010, 327, 1603-1607.
5. Kim, D. H.; Rogers, J. A. Stretchable electronics: materilas strategies and devices Adv. Mater. 2008, 20, 4887-4892.
6. Kim, D. H.; Ghaffari, R.; Lu, N.; Rogers, J. A. Flexible and stretchable electronics for biointegrated devices Annu. Rev. Biomed. Eng. 2012, 14, 113-128.
7. Sekitani, T.; Someya, T. Stretchable, large-area organic electronics Adv. Mater. 2010, 22, 2228-2246.
8. Kaltenbrunner, M.; Kettlgruber, G.; Siket, C.; Schwödiauer, R.; Bauer, S. Arrays of ultracompliant elecrochemical dry gel cells for stretchable electronics Adv. Mater. 2010, 22, 2065-2067.
9. Kaltenbrunner, M.; White, M. S.; Glowacki, E. D.; Sekitani, T.; Someya, T.; Sariciftci, N. S.; Bauer, S. Ultrathin and lightweight organic solar cells with high flexibility Nat. Commun. 2012, 3, 770.

10. Larson, C.; Peele, B.; Li, S.; Robinson, S.; Totaro, M.; Beccai, L.; Mazzolai, B.; Shepherd, R. Highly stretchable electroluminescent skin for optical signaling and tactile sensing Science 2016, 351, 1071-1074.
11. Rus, D.; Tolley, M. T. Design, Fabrication and control of soft robots Nature 2015, 521, 467-475.
12. Lipomi, D. J. Stretchable figures of merit in deformable elecronics Adv. Mater. 2016, 28, 4180-4183.
13. Choi, M. K.; Yang, J.; Kang, K.; Kim, D. C.; Choi, C.; Park, C.; Kim, S. J.; Chae, S. I.; Kim, T.; Kim, J. H.; Hyeon, T.; Kim, D. Wearable red-green-blue quantum dot light-emitting diode array using high-resolution intaglio transfer printing Nat. Commun. 2015, 6, 7149.
14. Wang, J.; Yan, C.; Chee, K. J.; Lee, P. S. Highly stretchable and sefl-deformable alternating current electroluminescent devices Adv. Mater. 2015, 27, 2876-2882.
15. Zhang, Z.; Guo, K.; Li, Y.; Li, X.; Guan, G.; Li, H.; Luo, Y.; Zhao, F.; Zhang, Q.; Wei, B.; Pei, Q.; Peng, H. A Colour-tunable, weavable fibre-shaped polymer light-emitting electrochemical cell Nat. Photonics 2015, 9, 233-238.
16. Chou, H. H.; Nguyen, A.; Chortos, A.; To, J. W. F.; Lu, C.; Mei, J.; Kurosawa, T.; Bae, W.; Tok, J. B. H.; Bao, Z. A Chameleon-inspired stretchable electronic skin with interactive color changing controlled by tactile sensing Nat. Commun. 2015, 6, 8011.
17. Tee, B. C.; Chortos, A.; Berndt, A.; Nguyen, A. K.; Tom, A.; McGuire, A.; Lin, Z. C.; Tien, K.; Bae, W.; Wang, H.; Mei, P.; Chou, H. H.; Cui, B.; Deisseroth, K.; Ng, T. N.; Bao, Z. A skin-inspired organic digital mechanoreceptor Science 2015, 350, 313-316.

18. Kim, D.; Lu, N.; Ma, R.; Kim, Y.; Kim, R.; Wang, S.; Wu, J.; Won, S. M.; Chung, H.; Keum, H.; McCormick, M.; Liu, P.; Zhang, Y.; Omenetto, F. G.; Huang, Y.; Coleman, T.; Rogers, J. A. Epidermal electronics Science 2011, 333, 838-844.
19. Wagner, S.; Bauer, S. Materials for stretchable electronics MRS Bull. 2012, 37, 207-213.
20. Lee, P.; Ham, J.; Lee, J.; Hong, S.; Han, S.; Suh, Y. D.; Lee, S. E.; Yeo, J.; Lee, S. S.; Lee, D.; Ko, S. H. Highly stretchable or transparent conductor fabrication by a hierarchical multiscale hybrid nanocomposite Adv. Funct. Mater. 2014, 5671–5678.
21. Park, Y. J.; Lee, S. K.; Kim, M. S.; Kim, H.; Ahn, J. H. Graphene-based conformal devices ACS Nano 2014, 8, 7655-7662.
22. Sekitani, T.; Nakajima, H.; Maedo, H.; Fukushima, T.; Aida, T.; Hata, K.; Someya, T. Stretchable active-matrix organic light-emitting diode display using printable elastic conductors Nat. Mater. 2009, 8, 494-499.
23. Chortos, A.; Koleilat, G. I.; Pfattner, R.; Kong, D.; Lin, P.; Nur, R.; Lei, T.; Wang, H.; Liu, N.; Lai, Y.; Kim, M.; Chung, J. W.; Lee, S.; Bao, Z. Mechanically durable and highly stretchable transistors employing carbon nanotube semiconductor and electrodes Adv. Mater. 2016, 28, 4441-4448.
24. Yu, Z.; Niu, X.; Liu, Z.; Pei, Q. Intrinsically stretchable polymer light-emitting devices using carbon nanotube-polymer composite electrodes Adv. Mater. 2011, 23, 3989-3994.
25. Liang, J.; Li, L.; Niu, X.; Yu, Z.; Pei, Q. Elastomeric polymer light-emitting devices and displays Nat. Photonics 2013, 7, 817-824.

26. Liang, J.; Li, L.; Tong, K.; Ren, Z.; Hu, W.; Niu, X.; Chen Y.; Pei, Q. Silver nanowire percolation network soldered with graphene oxide at room temperature and its application for fully stretchable polymer light-emitting diodes ACS Nano 2014, 8, 1590-1600.

27. White, M. S.; Kaltenbrunner, M.; Glowacki, E. D.; Gutnichenko, K.; Kettlgruber, G.; Graz, I.; Aazou, S.; Ulbricht, C.; Egbe, D. A. M.; Miron, M. C.; Major, Z.; Scharber, M. C.; Sekitani, T.; Someya, T.; Bauer, S.; Sariciftci, N. S. Ultrathin, highly flexible and stretchable PLEDs Nat. Photonics 2013, 7, 811-816.

28. Wagner, S.; Lacour, S. P.; Jones, J.; Hsu, P.; Sturm, J. C.; Li, T.; Suo, Z. Electronic skin: architecture and components Phys. E Low-Dimensional Syst. Nanostructures 2004, 25, 326-334.

29. Tang, J.; Li, J.; Vlassak, J.; Suo, Z. Adhesion between highly stretchable materials Soft Matter 2016, 12, 1093-1099.

30. Reineke, S.; Lindner, F.; Schwartz, G.; Seidler, N.; Walzer, K.; Lussern, B.; Leo, K. White organic light-emitting diodes with fluorescent tube efficiency Nature 2009, 459, 234-238.

31. Yan, G.; Wang, L.; Zhang, L. Recent research progress on preparation of silver nanowires by soft solution method, preparation of gold nanotubes and Pt nanotubes from resultant silver nanowires and their applications in conductive adhesive Rev. Adv. Mater. Sci. 2010, 24, 10-25.

32. So, F.; Kido, J.; Burrows, P. Organic light-emitting devices for solid-state lighting MRS Bull. 2008, 33, 663-669.

33. Pei, Q.; Yu, G.; Zhang, C.; Yang, Y.; Heeger, A. J. Polymer light-emitting electrochemical cells Science. 1995, 269, 1086-1088.

34. Tabatabaei, S. H.; Carreau P. J.; Ajji, A. Microporous membranes obtained from polypropylene blend films by stretching J. Membr. Sci. 2008, 325, 772-782.

35. Kim, Y.; Minami, N.; Kazaoui, S. Highly polarized absorption and photoluminescence of stretch-aligned single-wall carbon nanotubes dispersed in gelatin films Appl. Phys. Lett. 2005, 86, 073103.

36. Matyba, P.; Yamaguchi, H.; Eda, G.; Chhowalla, M.; Edman, L.; Robinson, N. D. Graphene and mobile ions: the key to all-plastic, solution-processed light-emitting devices ACS Nano 2010, 4, 637-642.

37. Shao, Y.; Bazan, G. C.; Heeger, A. J. Long-lifetime polymer light-emitting electrochemical cells Adv. Mater. 2007, 19, 365-370.

38. Yu, Z.; Sun, M.; Pei, Q. Electrochemical formation of stable p-i-n junction in conjugated polymer thin films J. Phys. Chem. B 2009, 113, 8481-8486.

39. Yu, Z.; Wang, M.; Lei, G.; Liu, J.; Li, L.; Pei, Q. Stabilizing the dynamic p-i-n junction in polymer light-emitting electrochemical cells J. Phys. Chem. Lett. 2011, 2, 367-372.

40. Malliaras, G.; Friend, R. An organic electronics primer Phys. Today 2005, 58, 53-58.

41. Yin, K.; Zhang, L.; Lai, C.; Zhong, L.; Smith, S.; Fong, H.; Zhu, Z. Photoluminescence anisotropy of uni-axially aligned electrospun conjugated polymer nanofibers of MEH-PPV and P3HT J. Mater. Chem. 2011, 21, 444-448.

42. Seitz, J. T. The estimation of mechanical properties of polymers from molecular structure J. Appl. Polym. Sci. 1993, 49, 1331-1351.

43. Dokukin, M. E.; Sokolov, I. On the measurements of rigidity modulus of soft materials in nanoindentation experiments at small depth Macromolecules 2012, 45, 4277-4288.

44. Young, T. J.; Monclus, M. A.; Burnett, T. L.; Broughton, W. R.; Ogin, S. L.; Smith, P. A. The use of the PeakForce quantitative nanomechanical mapping AFM-based method for high-resolution Young's modulus measurement of polymers Meas. Sci. Technol. 2011, 22, 125703.

45. Dokukin, M. E.; Sokolov, I. Quantitative mapping of the elastic modulus of soft materials with HarmoniX and PeakForce QNM AFM modes Langmuir 2012, 28, 16060-16071.

46. Schön, P.; Bagdi, K.; Molnár, K.; Markus, P.; Pukánszky, B.; Vancso, G. J. Quantitative mapping of elastic moduli at the nanoscale in phase separated polyurethanes by AFM Eur. Polym. J. 2011, 47, 692-698.

47. Hagler, T. W.; Pakbaz, K.; Voss, K. F.; Heeger, A. J. Enhanced order and electronic delocalization in conjugated polymers oriented by gel processing in polyethylene Phys. Rev. B 1991, 44, 8652-8666.

48. Dyreklev, P.; Berggren, M.; Inganäs, O.; Andersson, M. R.; Wennerström O.; Hjertberg, T. Polarized electroluminescence from an oriented substituted polythiophene in a light emitting diode Adv. Mater. 1995, 7, 43-45.

49. Friend, R. H.; Bradley, D. D. C.; Townsend, P. D. Photo-excitation in conjugated polymers J. Phys. D Appl. Phys. 1987, 20, 1367-1384.

50. Kim, J. B.; Kim, P.; Pégard, N. C.; Oh, S. J.; Kagan, C. R.; Fleischer, J. W.; Stone, H. A.; Loo, Y. Wrinkles and deep folds as photonic structures in photovoltaic Nat. Photonics 2012, 6, 327-332.

51. Wu, J.; Lu, X.; Yi, Z.; Shan, F.; Lu, Q. Anisotropic fluorescence emission of ionic complex induced by the orientation of azobenzene unit Macromolecules 2013, 46, 3376-3383.

# Chapter 4 A solid-state intrinsically stretchable polymer solar cell

## 4.1 Introduction

Fossil fuels are still providing the most consumed energy in the world right now. However, the scarcity of fossil resources, and the generation of greenhouse gas, such as carbon dioxide, put fuels into arguments. Renewable energy sources, including the wind, biomass, solar energy, and tide, are therefore of huge interest in an effort to alleviate the demand for fossil fuels and reduce greenhouse gas emission. Solar energy is an environmentally friendly and reliable resource. Efficient energy harvesting from the Sun and converting to electricity is one of the most attractive strategies by solar cells.

Solar cell technology falls into three categories. The first type of solar cells is fabricated on traditional silicon (Si) wafers, with a typical efficiency of 15-20% [1]. Si-based solar cells are still dominating the commercial solar market nowadays due to their high efficiency and stability. However, the rigid nature and high cost in Si production place major limits to the wide adoption. The second type of solar cells is thin-film solar cells, including amorphous silicon (a-Si), copper indium gallium selenide (CIGS), and cadmium telluride (CdTe), with a typical efficiency between 10-15%. The thickness reduction in thin-film solar cell improves the flexibility of the entire device. However, the aforementioned inorganic materials belong to scarce elements, and high temperature and high vacuum are necessary during the fabrication process with these materials, leading to an unnegligible energy consumption. Besides, toxic chemicals, such as cadmium, are used in the production process, bringing danger to health and to the environment [2]. Organic photovoltaics (OPVs) are referred to as the third generation of

solar cells, and power conversion efficiency of 11.5% has been achieved in a single junction organic solar cell [3]. The raw materials used in OPVs are earth abundant and light weighted. Mechanical compliance is often expected as such thin devices can bear bending with a curvature as small as 1 mm in radius without cracking caused by the large strain [4-6]. Thus OPVs could be used to replace conventional rigid solar cells and be mounted on curved surface, portable and wearable electronics, or even moving parts of machinery and robots due to their mechanical flexibility and solution processability [7].

Polymer light emitting diodes and polymer electrochemical cells consisting emissive layer sandwiched between stretchable and transparent electrodes could be stretched as much as 140% [8-10]. However, large strain deformation is still a major challenge posed to materials and device operation. Few efforts have been made to OPV devices which could withstand large-strain deformation. A fundamental understanding on the mechanical deformation of such stretchable solar cells will provide an insight view on OPV performance and may lead to a general approach to impart elasticity to OPV materials which are otherwise brittle.

## 4.2 Experimental methods

***Electrode preparation*.** Successively coating a layer of functionalized single wall carbon nanotube (SWNT, Carbon Solutions, Inc.) and a layer of silver nanowire (AgNW, synthesized according to a literature procedure [11]) from respective dispersions on glass substrate at ambient temperature and pressure formed a bilayer AgNW/SWNT electrode on the glass substrate. The AgNW has an average diameter in the range of 25-35 nm and average length between 10-20 μm. A polymer precursor solution containing urethane acrylate oligomer (UA,

Sartomer USA), ethoxylated bisphenol A dimethacrylate (EBA, Sartomer USA), and 2,2-dimethoxy-2-phenylacetophenone (Sigma-Aldrich) with a weight ratio of 100:20:1 was deposited on the as-prepared AgNW/SWNT bilayer on glass substrate. The precursor coating was cured on a Dymax ultraviolet curing conveyor equipped with a 2.5 W/cm$^2$ Fusion 300S type 'H' ultraviolet curing bulb and then peeled off as a free-standing composite electrode. The resulting composite electrode is denoted as SWNT/AgNW-PUA.

***Organic solar cell (OPV) sample preparation*.** SWNT/AgNW-PUA composite stretchable electrode with sheet resistance of 10 ohm/□ was used as transparent electrode. The electrode was cleaned by sequential 30 min treatments with detergent followed by deionized water in an ultrasonic bath. Poly(3,4-ethylenedioxythiophene):poly(styrenesulfonate) (PEDOT:PSS, Clevios VP Al 4083 from H. C. Starck Inc.) was spin-coated on a composite electrode at 4000 rpm for 60 s, followed by drying in a vacuum chamber for 24 h to remove residual water. Onto the coated electrode, a solution containing poly(thieno[3,4-b]-thiophene/benzodithiophene) (PTB7, 1-material Inc.) and [6,6]-phenyl-$C_{71}$-butyric acid methyl ester ($PC_{71}BM$, Sigma-Aldrich, 99%) dissolved in chlorobenzene (CB) and 1,8-diiodoctane (DIO) (97:3 wt%) as the mixture solvent was spin-coated at 900 rpm for 60 seconds. The weight ratio of PTB7:$PC_{71}BM$ was 1:1.5, and the thickness of blend film was 140 nm measured by Dektak 6 Surface Profilometer. On a second composite electrode, a solution of ethoxylated polyethylenimine (PEIE, Mw=75,000 g/mol, Sigma-Aldrich) dissolved in 2-methoxyethanol to 0.4 wt% concentration was spin-coated at 5000 rpm for 60 s. The PEIE coating was then dried in a vacuum chamber at ambient temperature. The thickness of the PEIE layer was around 5 nm. Finally, the as-prepared PEIE/composite electrode and PTB7:$PC_{71}BM$/PEDOT:PSS/composite

electrode were laminated with the active materials facing each other, and heated to 100 ℃ for 3 min to afford strong adhesion. The lamination was done in a nitrogen protected glovebox, with oxygen and moisture levels below 0.1 ppm. The photosensitive area of the freshly prepared devices was 0.12 $cm^2$.

***Sample preparation.*** A solution of PTB7, $PC_{71}BM$, DIO in CB (weight ratio 100:150:3) was spin-coated at 900 rpm for 60s onto the pre-crosslinked ClearFlex 50 (ClearFlex50, mixed at a weight ratio of 1:1 parts A:B, Smooth-On USA) substrate. The film was then dried under vacuum overnight to remove residue CB and DIO.

***Characterization.*** UV-vis absorbance spectra were collected by Shimadzu UV-1700 spectrophotometer. AFM measurements were carried out in PeakForce QNM (Quantitative NanoMechanics) mode on a Bruker dimension icon scanning probe microscope at ambient conditions. A commercial silicon cantilever (MPP-11120) was used. The typical radius of curvature is ~8 nm and a nominal spring constant is ~40 N/m. QNM mapping had constant peak force during operation. Current density-voltage (J-V) were measured by a Keithley 2400 Semiconductor Characterization System. The photovoltaic performance was measured under an air mass of a 1.5 solar illumination at 100 $mW/cm^2$ (1 sun). All device performance measurements were carried out at room temperature in the glovebox.

## 4.3 Results and Discussion

### 4.3.1 Stretchable OPV device

An electron-rich donor, poly(thieno[3,4-b]-thiophene/benzodithiophene) (PTB7), and an electron-deficient moieties acceptor, phenyl-C71-butyric acid methyl ester ($PC_{71}BM$) blend

film is studied here. Since C70 derivatives have stronger phosphorescence than C60 derivatives owing to the less symmetrical structure in $PC_{71}BM$, which have more optical transition states [12], power conversion efficiency (PCE) based on PTB7:$PC_{71}BM$ blend is reported to be higher than 8% [13]. The use of high boiling point 1,8-diiodooctane (DIO, b.p. 365℃/ 760 mmHg) has a profound impact on the PCE of PTB7:$PC_{71}BM$ blend, by increasing both short-circuit current density (Jsc) and fill factor (FF) [14]. In an unpublished work, an intrinsically stretchable solar cell with a photovoltaic blend film of PTB7:$PC_{71}BM$:DIO sandwiched between a pair of transparent electrodes had been demonstrated (Figure 4.1a). Each of the transparent electrodes is composed of a stack of a silver nanowire (AgNW) percolation network and a single wall carbon nanotube (SWNT) network. Poly(3,4-ethylenedioxythiophene): poly(styrenesulfonate) (PEDOT:PSS) and ethoxylated polyethylenimine (PEIE) are used as interfacial layer inserted on top of the anode and cathode respectively, to enhance hole and electron extraction. The use of DIO significantly improved the PCE, from 1.79% without DIO to 3.45% (Figure 4.1c). The efficiency is lower than that from the standard device (8%) [15], which should take the transparency of both electrodes into consideration since traditional OPV devices have reflective metallic cathode. The OPV device with DIO could withstand strain as much as 100%. PCE of PTB7:$PC_{71}BM$ diminished to only 0.3% with only 10% strain (Figure 4.1b). The laminated OPV with DIO deforms without sacrificing too much of its performance at room temperature at small strain. PCE even shows a slight increase with stretching up to 30% strain. A summary of OPV processed with CB/DIO performance is listed in Table 4.1. The buckled surface caused by stretching-relaxation could be the reason that leads to the increased $J_{SC}$. The enhanced effective light paths from buckled surface will attribute to the photon

absorption by redirecting them into the absorbing active layer [16], and will be discussed in section 4.3.3. Meanwhile, the rough surface may lead to increased possible leakage pathways, thus decreases the FF. The change in the interfaces at OPV blend and electrodes could also be a factor to improve charge collection at the stretching states [17,18].

### 4.3.2 Bulk heterojunction formation

The primary function of solar cells is to convert solar energy into electrical energy by photovoltaic effect. In organic photovoltaics, the electron-hole pair is created by absorbing photons and is held together by Coulomb forces. In order to generate electricity, the electrons and holes need to be separated and collected at the cathode and anode respectively. A conjugated polymer with a higher lowest unoccupied molecular orbital level is used as the electron donor and absorbs photon. Fullerene or n-type polymer is used to acquire electron and is called electron acceptor [19-22].

Exciton has a short lifetime, and the distance between the interface of donor/acceptor and exciton generation site is about 10 nm in a typical OPV. Meanwhile, the electrons and holes should have their own diffusion path to the respective electrode where they are collected. Three types of donor and acceptor mixture morphology are elaborated in Figure 4.2. The interface between donor and acceptor effectively prevents charges from running into the opposite electrode in the bilayer structure (Figure 4.2a). The comb structure in Figure 4.2b has a large interfacial contact area and could efficiently separate electronic charges. But it is difficult to manipulate such morphology by solution process. Bulk heterojunction (BHJ) is more commonly seen as a mixture of donor and acceptor, and has a binary phase segregated

morphology with the domain size of the order of 10 nm [15]. The percolation structure boosts larger interfacial area, and forms continuous pathways for electrons and holes to move towards respective electrode. This BHJ morphology is critical for efficient exciton dissociation and charge transportation to achieve high efficiency solar cell.

To study the influence of deformation on OPV morphology, a transparent stretchable polyurethane rubber, ClearFlex 50 (500% elongation at break), was chosen as elastomeric substrate. PEDOT:PSS was spin-coated on the substrate surface to 1) protect polyurethane from solvent attack in the subsequent coating of OPV active layer, and 2) be consistent with the OPV device architecture which would more accurately reflect how the donor and acceptor are agglomerated. The OPV blend film was 100 nm in thickness.

The height and phase image of the OPV blend was imaged by tapping mode AFM. Large scale domains of around 100-200 nm in diameter are found in the PTB7:$PC_{71}BM$ blend film (Figure 4.3a and b). The large domains are not favored for exciton migration to the donor/acceptor interface, nor for the resistance to mechanical strain. On the other hand, the usage of DIO has a profound impact on reducing phase separation in the OPV blend film. The fresh blend film using DIO additive in CB shows smaller grain size (Fig 4.3c and d). Small domains around tens of nanometers are necessary to enlarge the interfacial contact area to increase the probability of exciton dissociation and charge collection, and thus improve device efficiency as implied in Table 4.1. The distance between neighboring $PC_{71}BM$ domains is reduced so that the molecular connectivity is improved, and the electron mobility is increased [23]. These AFM morphologies are also in consistence with the transmission electron microscopic (TEM) images obtained by Yu et al. [13,24].

Large cracks were developed on PTB7:$PC_{71}BM$ film at only 10% strain, leading to the failure of entire device. However, with 50% strain applied to the PTB7:$PC_{71}BM$ film processed with DIO, no observable cracks or broken lines were introduced. A slight preferential alignment at around 45 degrees along axis of strain direction is shown as in Figure 4.4c, where a randomly oriented profile is presented in the as-formed film.

PeakForce Quantitative NanoMechanical (QNM) mapping is used to generate surface quantitative mechanical properties mapping [25, 26]. The contrast reflects different Young's modulus derived from the force-distance curve recorded [27]. Here, we used PeakForce QNM mapping mode at ambient condition to examine the morphology of PTB7:$PC_{71}BM$ blend films and to measure the surface Young's modulus distribution mapping information. OPV blend film was coated on a glass slide with a pre-coating PEDOT:PSS layer. Figure 4.5a is QNM mapping image of a PTB7:$PC_{71}BM$ film. Young's modulus mapping of the PTB7:$PC_{71}BM$ again reveals major phase separation. The Young's modulus value of the continuous phase in darker color is 7.0±0.8 GPa. The isolated domains in lighter color are much stiffer, with a modulus value of around 12±1.0 GPa. Since neat PTB7, and neat $PC_{71}BM$ has a reported Young's modulus at the value of ~1.1 GPa and ~3.1 GPa [28, 29], the continuous phase shown in Fig 5a is mainly PTB7 while the large domains are $PC_{71}BM$. The addition of $PC_{71}BM$ into PTB7 dramatically increases Young's modulus value in the composite materials about 5 times due to the filler effect of $PC_{71}BM$ nanoparticles [30, 31]. Continuously and smoothly distributed surface modulus mapping feature can be found in Figure 4.5b, the film of which was processed with DIO. The Young's modulus is 9.5±0.5 GPa in the brighter regime and 5.5±0.5 GPa in the darker area. DIO additive plasticized PTB7:$PC_{71}BM$ by reducing the

stiffness of PTB7:$PC_{71}BM$ blend film. We did not measure precise Young's modulus information on the DIO processed PTB7:$PC_{71}BM$ blend film under deformation. The average spring constant of the cantilever probe used here is ~40 N/m, and the large spring constant probe could not provide enough reliable force-distance curves since the indentation into the surface is too small. Methods to soften the cantilever into proper frequency to be adapted to this rigid material embedded in a soft substrate is necessary.

### 4.3.3 Dichroism of optical absorption

Figure 4.6 is the absorbance spectra of the OPV blend film under different strain rates during one stretching-relaxation cycle measured by ultraviolet-visible (UV-vis) absorption spectroscopy. The absorption spectrum shows that the OPV mixture has a peak of photosensitizing PTB7 at 680 nm, and a negligible absorption beyond 760 nm. The other peak at 460 nm is the indication of $PC_{71}BM$. The addition of DIO did not shift peak position. The peak absorption intensity decreases from 0 to 100% strain. The decreased thickness of the active layer during stretching can reduce the absorption peak intensity. When relaxed back to 0% strain, the absorbance intensity values are higher than that of the fresh film, in consistent with the theory that the formation of nanosized buckles leads to increased light path in the corrugated structure [16]. OPV with DIO could be stretched as much as 100%. No visible delamination, or crack was observed from repeated stretching-relaxation in the PTB7:$PC_{71}BM$ sample processed with DIO.

Polymer semiconductors have the property that optical transition dipole moment ($\pi$-$\pi$*) can be aligned along the polymer backbone [32, 33]. And thus the uniaxially aligned polymer

film results in anisotropic optoelectronic properties [34-36]. Polarized optoelectronic behavior under mechanical deformation has been investigated, by placing a McMaster Carr. polarizing prism (~0.006" in thickness) between the photoluminescence detector and the sample so that only light from selected direction was collected. The absorption spectra of OPV blend measured with linearly polarized light parallel and perpendicular to the strain direction (defined as "para" and "perp" direction), are provided in Figure 4.7. The films were strained from 0% to 100%, with 25% increments. No polarization is observed from neither sample at 0% strain. When strain was applied, the absorption intensity is enhanced in the strain direction, and reduced in the orthogonal direction which is consistent with the fact that conductivity and field-effect mobility is enhanced in the stretching direction in conductive polymers [34-38]. The anisotropic PTB7 peak absorption as the strain increased in OPV blends indicates in-plane alignment, which is in accordance with strain-aligned neat PTB7 films.

Although the polarized absorption shows anisotropic behavior under strain in both samples, absorption dichroism is different when strain is released. In OPV blend processed with DIO, the absorbance spectra are higher than that of the fresh film in both parallel and perpendicular direction due to the increased light path from corrugated structure when film is relaxed to 0% strain; and the spectra in orthogonal directions coincide with each other (Figure 4.8). On the contrary, in PTB7:$PC_{71}BM$ sample, UV-abs spectra intensity at parallel direction are higher than perpendicular direction when the strain was removed (Figure 4.9).

Dichroic ratio (DR), defined in equation (1), is taken as absorbance of light polarized parallel to the strain direction to absorbance of light polarized perpendicular to the strain direction. DR value is an indicator of alignment of conjugated polymer backbone in response

to the strain.

$$\mathrm{DR} = \frac{Abs_{//}}{Abs_{\perp}} \qquad (1)$$

Where $Abs_{//}$ and $Abs_{\perp}$ are the absorbance value at parallel and perpendicular direction. In this OPV blend study, DR values are calculated from the absorbance at wavelength of 680 nm and 460 nm separately, using the ratio of maximum polarized absorbance value parallel to the strain direction to perpendicular to the strain direction. The dichroic ratio is summarized at 680 nm and 460 nm separately in Figure 4.10 and Table 4.2. Dichroism from strained neat PTB7 and $PC_{71}BM$ film shows the limiting factor to PTB7:$PC_{71}BM$ film. Dichroism seen in PTB7:$PC_{71}BM$ sample is in agreement with the widely reported molecular alignment of conjugated polymers along the stretching direction, where photoluminescence and electroluminescence are polarized along the elongated axis [39,40]. These results show that PTB7:$PC_{71}BM$ is not stretchable due to high glass transition temperature [41]. Large $PC_{71}BM$ domains further stiffen the OPV blend. The dichroism after strain is relaxed also indicates the irreversible plastic deformation nature in PTB7:$PC_{71}BM$ blend film.

In PTB7:$PC_{71}BM$:DIO blend film, dichroism is observed only during stretching at orthogonally polarized direction. The anisotropic polarization behavior under strain is most likely due to the alignment of crystalline PTB7 within grains, leading to a lower density of polymer chains entanglement. The deformation of both PTB7 and $PC_{71}BM$ are reversible as absorption spectra indicated in Figure 4.9. DR is ~1.00, fluctuating in a fairly narrow range of ±3%, after relaxed from each strain rate. Small grains in this film help to accommodate reversible deformation by relative motion towards each other, and no dramatic changes occurred to the optoelectronic properties when strain is released.

AFM shows that there are large domains (~100-200 nm in diameter) in the OPV blend film without DIO, resulting in the poor ductility in the BHJ active layer. $PC_{71}BM$ in the blend film makes the film more brittle. This OPV film has the tendency to crack at low value of elongation (10%), characteristic of the brittle nature.

On the other hand, the PTB7:$PC_{71}BM$ blend containing 3 wt% DIO shows a morphology of uniform dispersion of much smaller grains than in the blends without DIO, indicating improved mixing between PTB7 and $PC_{71}BM$ from AFM. The high boiling point DIO added in the blend solution not only improves the miscibility between PTB7 and $PC_{71}BM$ and thus reduced grain size, its much higher boiling point (365 ℃/ 760 mmHg) or lower vapor pressure than that of the chlorobenzene also indicates that the DIO leaves the blend film when the film has already formed its solid state. The vaporization of DIO thus leaves behind free volumes which are critical to the enhanced deformability of the solid state film. A substantial amount of external strain energy could be translated into relative sliding and re-orientation of the nano-grains, as beach sand. The conjugated polymer chains are locally re-oriented with the grains in the crystallinity region, but no net re-orientation of the chains globally. The deformation thus does not cause dramatic alteration of the electronic and photonic properties of the blend film, and the deformation is reversible. The deformation is largely reversible as the nano-grains can slide back as the blend film contracts with the elastomeric substrate. A schematic overview of such phase morphology in response to strain is represented in Figure 4.10.

## 4.4 Summary

In summary, an intrinsically stretchable OPV has been demonstrated. The use of the high

boiling point additive DIO not only enhance the miscibility of PTB7 and $PC_{71}BM$, but also creates free volume in the blend after evaporation of DIO during the device fabrication process. Prior studies have shown that the nanometer-size, uniform grains of the intimating mixture of $PC_{71}BM$ in PTB7 can overcome the limitation of exciton diffusion length, as the distance electrons have to hop from grain to grain till being collected on the electrode is significantly reduced due to the reduction of grain size. Meanwhile, the free volume in the blend enhances the stretchability of PTB7:$PC_{71}BM$ mixture which could thus withstand elastic deformation up to 100% at room temperature.

## 4.5 Figures

Figure 4.1 (a) Schematic illustration of the sandwich structure of an elastomeric OPV. J-V characteristics of the OPV based on (b) PTB7:$PC_{71}BM$, and (c) PTB7:$PC_{71}BM$:DIO [Unpublished work, from Dr. Lu Li].

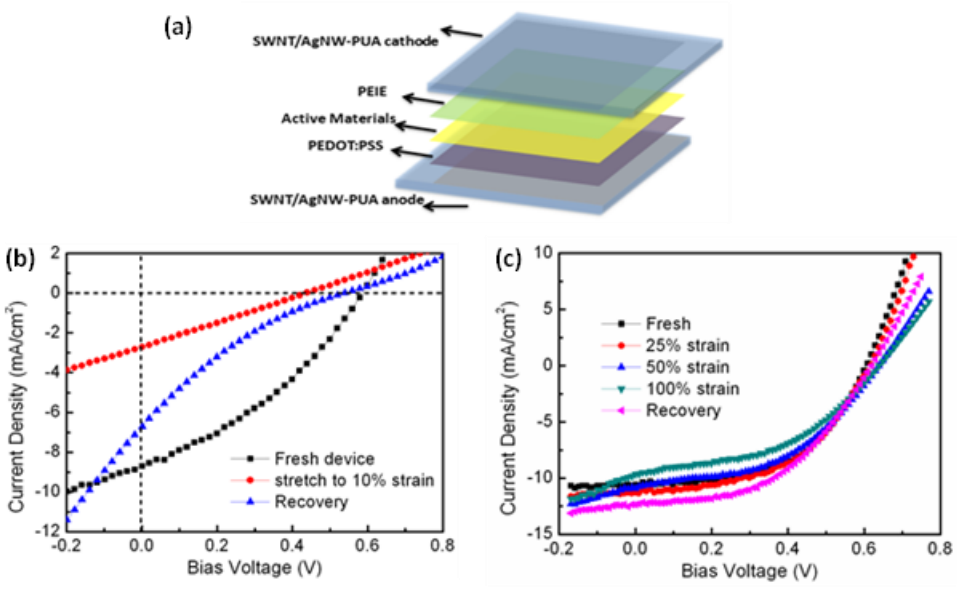

Figure 4.2 Three types of blending electron donor and acceptor morphology. (a) Bilayer structure; (b) comb structure; (c) solution processed randomly phase separation structure (BHJ).

Figure 4.3 Top surface morphology of PTB7:$PC_{71}BM$ (1:1.5) blends processed from CB (a, b) and CB/DIO mixture (c, d) at 0% strain. (a) and (c) are height images; (b) and (d) are phase images.

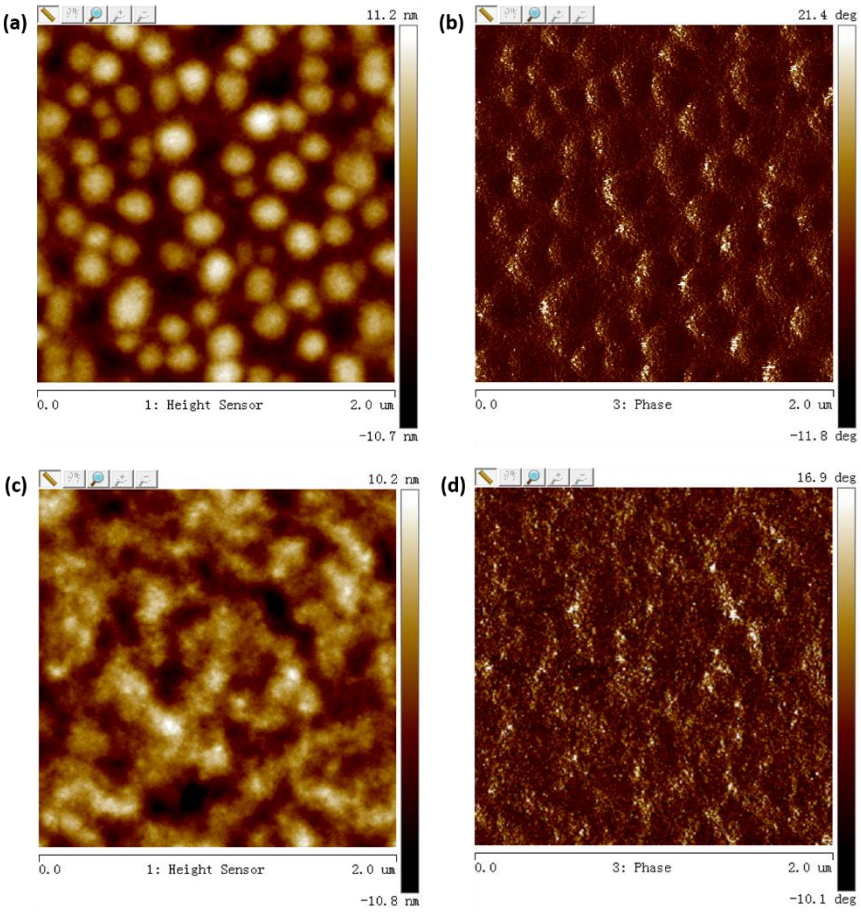

Figure 4.4 Top surface morphology of PTB7:$PC_{71}BM$:DIO (1:1.5:3%) blends at (a, b) 0% strain and (c,d) 50% strain. (a) and (c) are height images; (b) and (d) are phase images.

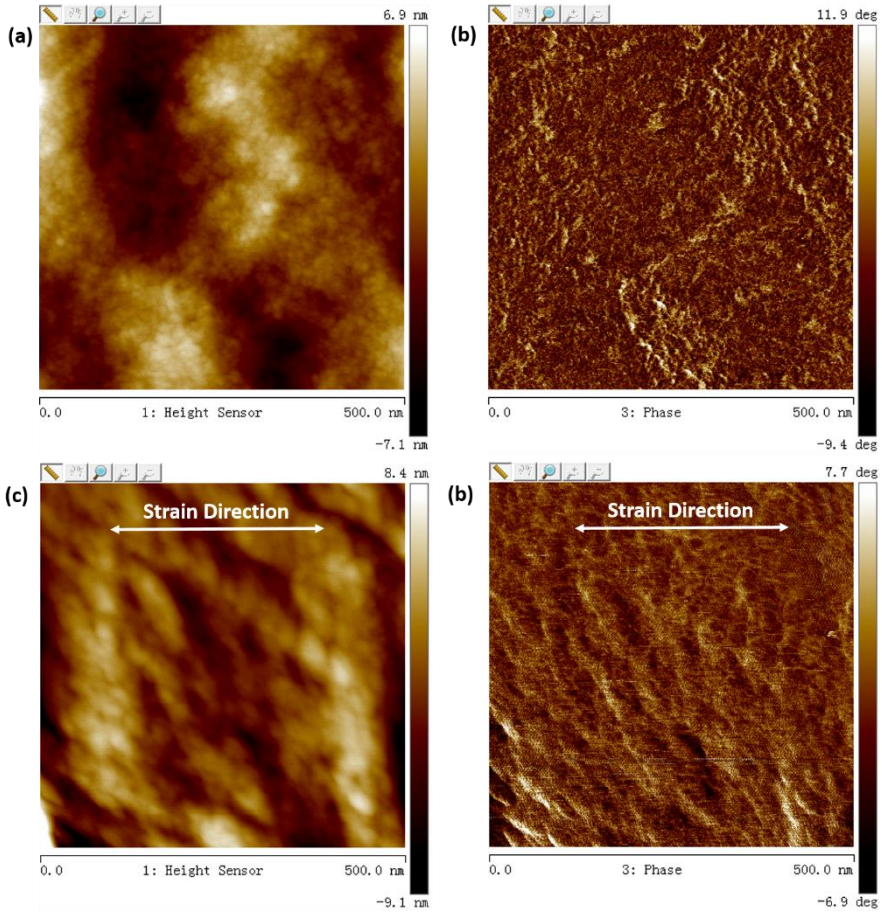

Figure 4.5 PeakForce QNM Young's modulus mapping of PTB7:$PC_{71}BM$ (1:1.5) blends processed from (a) CB and (b) CB/DIO at 0% strain.

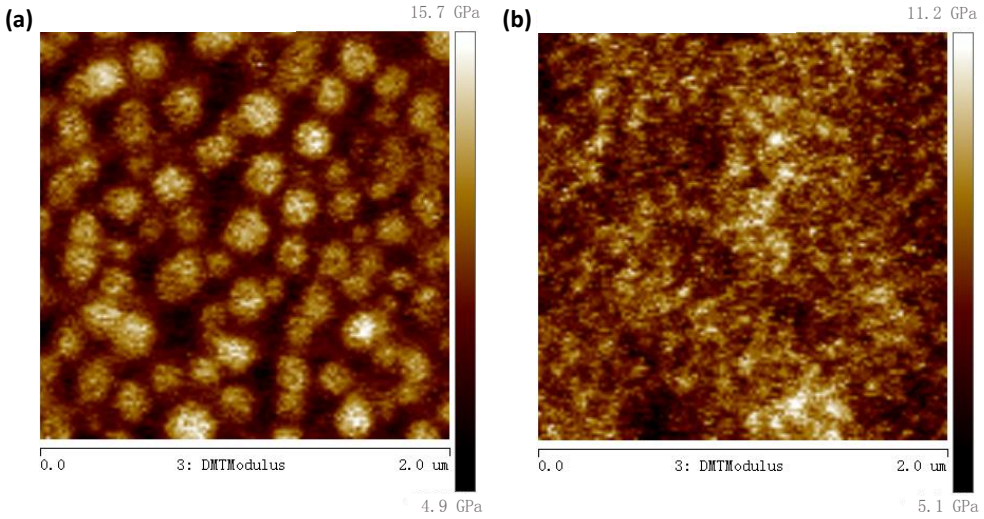

Figure 4.6 UV-vis absorbance spectra for strain aligned (a) PTB7:$PC_{71}BM$ and (b) PTB7:$PC_{71}BM$:DIO (3 wt%) blend films; relaxed from strained film of (c) PTB7:$PC_{71}BM$, and (d) PTB7:$PC_{71}BM$:DIO (3 wt%).

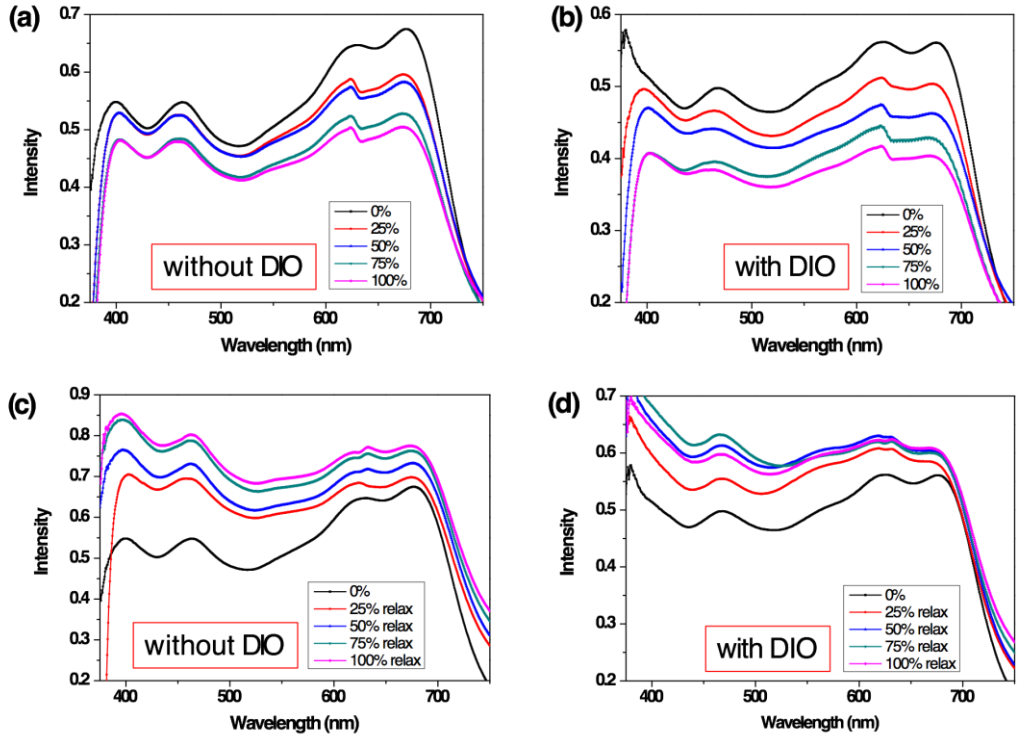

Figure 4.7 UV-vis absorbance spectra for strain aligned (a) PTB7:$PC_{71}BM$ and (b) PTB7:$PC_{71}BM$:DIO (3 wt%) blend films, (c) PTB7, and (d) $PC_{71}BM$ film with incident light polarized parallel (para) and perpendicular (perp) to the strain direction.

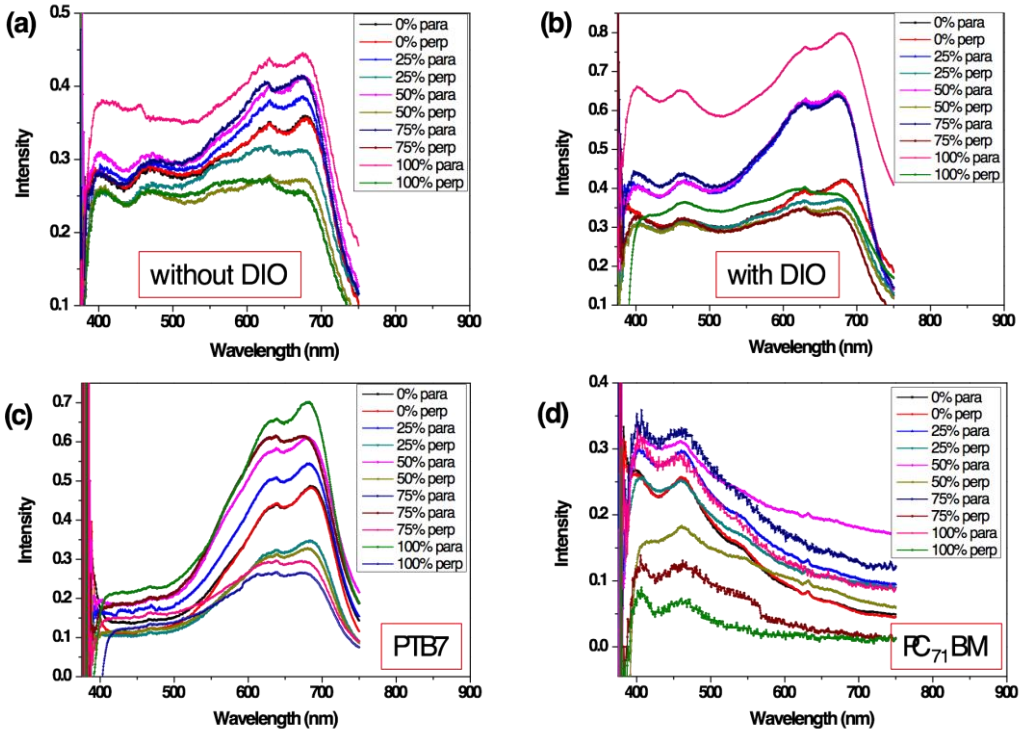

Figure 4.8 Isotropic UV-vis absorbance spectra of PTB7:$PC_{71}BM$:DIO (3 wt%) released from certain strain (25, 50, 75, and 100%) as is denoted in the figures, with incident light polarized parallel (para) and perpendicular (perp) to the strain direction.

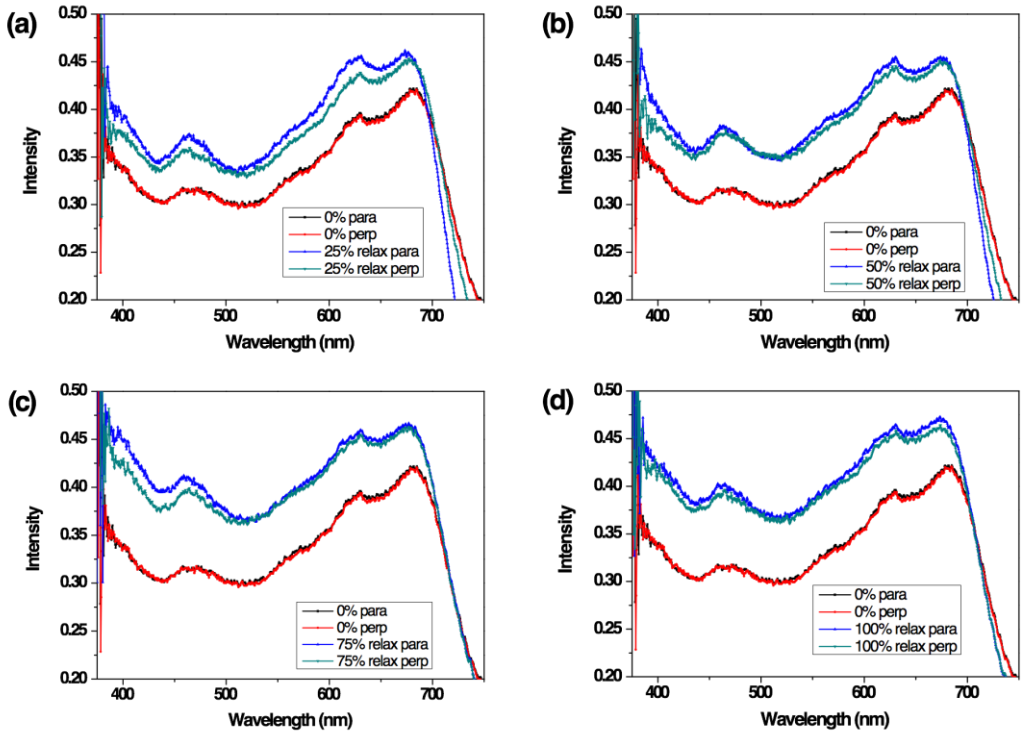

Figure 4.9 Anisotropic UV-vis absorbance spectra of PTB7:$PC_{71}BM$ released from certain strain (25, 50, 75, and 100%) as is denoted in the figures, with incident light polarized parallel (para) and perpendicular (perp) to the strain direction.

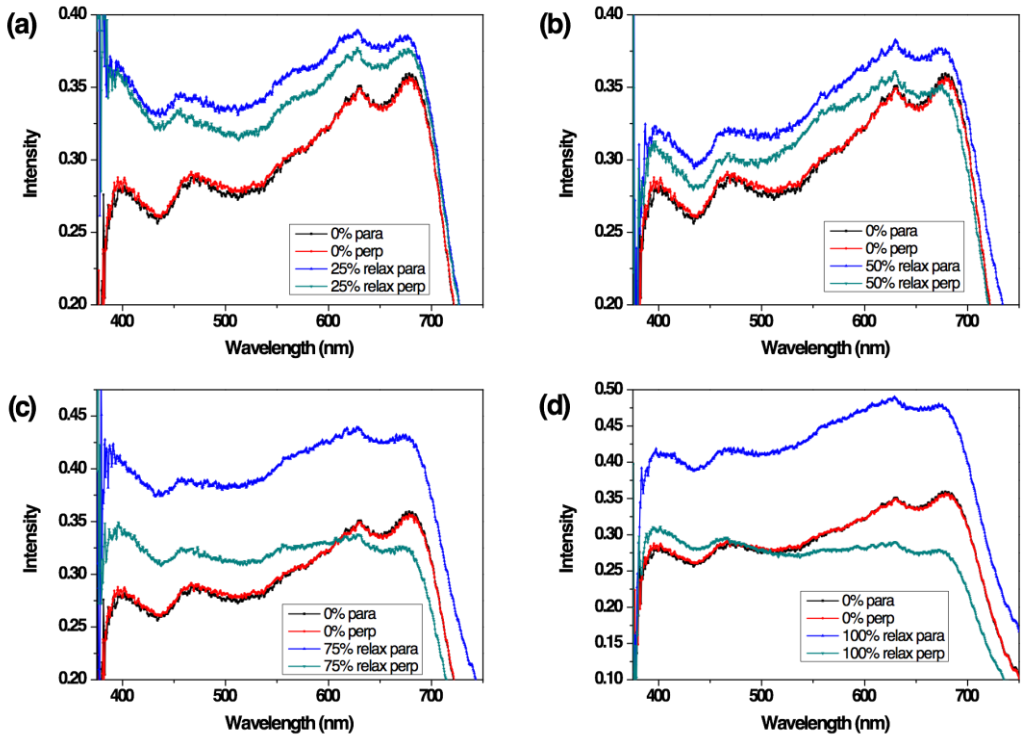

Figure 4.10 Schematic view of the phase morphology of OPV blend film processed with DIO in response to uniaxial stretching.

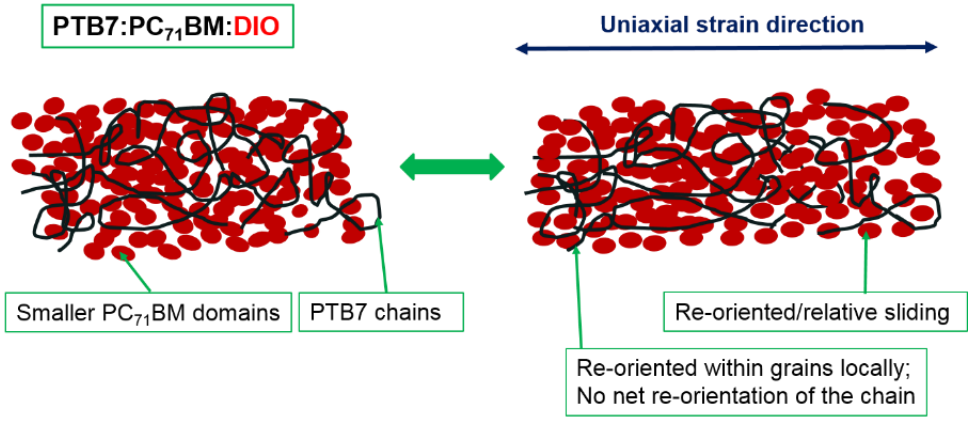

Table 4.1 Photovoltaic parameters for OPVs processed with CB/DIO at different stretching strains [Unpublished work, from Dr. Lu Li].

| Strain | $I_{SC}$ (mA) | $J_{SC}$ ($mA/cm^2$)[a] | FF | $V_{OC}$ (V) | $P_{max}$ (mW) | PCE (%) |
|---|---|---|---|---|---|---|
| 0% | 0.40±0.03 | 9.9±0.7 | 0.51±0.04 | 0.58±0.02 | 0.13±0.01 | 2.9±0.06 |
| 25% | 0.50±0.04 | 10.3±0.8 | 0.50±0.05 | 0.59±0.02 | 0.16±0.01 | 2.9±0.7 |
| 50% | 0.55±0.04 | 9.9±0.8 | 0.42±0.05 | 0.62±0.03 | 0.16±0.01 | 2.6±0.6 |
| 100% | 0.56±0.06 | 8.6±0.9 | 0.41±0.05 | 0.61±0.03 | 0.16±0.02 | 2.1±0.6 |
| Recovery | 0.45±0.04 | 11.2±1.1 | 0.44±0.05 | 0.60±0.02 | 0.12±0.01 | 3.0±0.7 |

$I_{sc}$ : Short Circuit Current; FF: Fill factor; $V_{oc}$ :Open Circuit Voltage; $P_{max}$ :Maximum Power

[a)] The active area of the unstretched cells is 4 $mm^2$.

Table 4.2 DR ratio calculated from UV-abs spectra of PTB7:$PC_{71}BM$ and PTB7:$PC_{71}BM$:DIO blend samples at 680 nm and 460 nm separately.

| Strain | Dichroic Ratio | | | | | | | |
|---|---|---|---|---|---|---|---|---|
| | PTB7:$PC_{71}BM$ | | | | PTB7:$PC_{71}BM$:DIO | | | |
| | 460 nm | | 680 nm | | 460 nm | | 680 nm | |
| | S | R | S | R | S | R | S | R |
| 0% | 1.00 | | 1.00 | | 1.00 | | 1.00 | |
| 25% | 1.10 | 1.03 | 1.23 | 1.02 | 1.33 | 1.04 | 1.73 | 1.02 |
| 50% | 1.20 | 1.06 | 1.52 | 1.11 | 1.35 | 1.01 | 1.84 | 1.01 |
| 75% | 1.16 | 1.20 | 1.61 | 1.32 | 1.36 | 1.03 | 1.89 | 1.01 |
| 100% | 1.45 | 1.42 | 1.74 | 1.72 | 1.79 | 1.01 | 2.09 | 1.01 |

*S: being stretched

*R: relaxed from strain

## 4.6 Reference


1. http://plasticphotovoltaics.org/lc/lc-solarcells/lc-introduction.html
2. http://www.energybc.ca/cache/solarpv/www.cetonline.org/Renewables/PV_pro_con.html
3. Zhao, J.; Li, Y.; Yang, G.; Jiang, K.; Lin, H.; Ade, H.; Ma, W.; He, Y. Efficient organic solar cells processed from hydrocarbon solvents Nat. Energy 2016, 2, 15027.
4. Brand, V.; Bruner, C.; Dauskardt, R. H. Cohesive device reliability in organic bulk heterojunction photovoltaic cells Solar Energy Materials & Solar Cells 2012, 99 182–189.
5. Dupont, S. R.; Oliver, M.; Krebs, F. C.; Dauskardt, R.H. Interlayer adhesion in roll-to-roll processed flexible inverted polymer solar cells Solar Energy Materials & Solar Cells. 2012, 97, 171–175.
6. Suo, Z.; Ma, E. Y.; Gleskova, H.; Wagner, S. Mechanics of rollable and foldable film-on-foil electronics Appl. Phys. Lett. 1999, 74, 1177–1179.
7. Gunes, S.; Neugebauer, H.; Sariciftci, N. Conjugated polymer-based organic solar cells Chem. Rev. 2007, 107, 1324–1338.
8. Sekitani, T.; Nakajima, H.; Maedo, H.; Fukushima, T.; Aida, T.; Hata K.; Someya, T. Stretchable active-matrix organic light-emitting diode display using printable elastic conductors Nat. Mater. 2009, 8, 494-499.
9. Liang, J.; Li, L.; Tong, K.; Ren, Z.; Hu, W.; Niu, X.; Chen, Y.; Pei, Q. Silver nanowire percolation network soldered with graphene oxide at room temperature and its application for fully stretchable polymer light-emitting diodes ACS Nano 2014, 8, 1590-1600.
10. Gao, H.; Chen, S.; Liang, J.; Pei, Q. Elastomeric light emitting polymer enhanced by interpenetrating networks ACS Appl. Mater. Interfaces 2016, 8, 32504-32511.

11. Yang, C.; Gu, H.; Lin, W.; Yuen, M. M.; Wong, C. P.; Xiong, M.; Gao, B. Silver nanowires: from scalable synthesis to recyclable foldable electronics Adv. Mater. 2011, 23, 3052-3056.
12. Wasielewski, M. R.; O'Neil, M. P.; Lykke, K. R.; Pellin, M. J.; Gruen, D. M. Triplet states of fullerenes C60 and C70 electron paramagnetic resonance spectra, photophysics, and electronic structures J. Am. Chem. Soc. 1991, 113, 2774 -2776.
13. Liang, Y.; Xu, Z.; Xia, J.; Tsai, S. T.; Wu, Y.; Li, G.; Ray, C.; Yu, L. For the bright future-bulk heterojunction polymer solar cells with power conversion efficiency of 7.4% Adv. Mater. 2010, 22, E135-E138.
14. He, Z.; Zhong, C.; Su, S.; Xu, M.; Wu, H.; Cao, Y. Enhanced power-conversion efficiency in polymer solar cells using an inverted device structure Nat. Photon. 2012, 6, 591-595.
15. Scharber, M. C.; Muehlbacher, D.; Koppe, M.; Denk, P.; Waldauf, C.; Heeger, A. J.; Brabec, C. J. Design rules for donors in bulk-heterojunction solar cells-towards 10% energy-conversion efficiency Adv. Mater. 2006, 18, 789-794.
16. Kim, J. B.; Kim, P.; Pegard, N. C.; Oh, S. J.; Kagan, C. R.; Fleischer, J. W.; Stone, H. A.; Loo, Y. L. Wrinkles and deep folds as photonic structures in photovoltaics Nat. Photon. 2012, 6, 327-332.
17. Zhou, Y.; Fuentes-Hernandez, C.; Shim, J.; Meyer, J.; Giordano, A. J.; Li, H.; Winget, P.; Papadopoulos, T.; Cheun, H.; Kim, J.; Fenoll, M.; Dindar, A.; Haske, W.; Najafabadi, E.; Khan, T. M.; Sojoudi, H.; Barlow, S.; Graham, S.; Brédas, J.; Marder, S. R.; Kahn, A.; Kippelen, B. A universal method to produce low-work function electrodes for organic electronics Science 2012, 336, 327-332.
18. He, Z.; Zhong, C.; Huang, X.; Wong, W. Y.; Wu, H.; Chen, L.; Su, S.; Cao, Y.

Simultaneous enhancement of open-circuit voltage, short-circuit current density, and fill factor in polymer solar cells Adv. Mater. 2011, 23, 4636-4643.

19. Gregg, B. Excitonic solar cells J. Phys. Chem. B 2003, 107, 4688–4698.
20. Tang, C. Two-layer organic photovoltaic cell Appl. Phys. Lett. 1986, 48, 183.
21. Spanggaard, H.; Krebs, F. A brief history of the development of organic and polymeric photovoltaics Sol. Energ. Mat. Sol. Cells 2004, 83, 125–146.
22. Li, G.; Zhu, R.; Yang, Y. Polymer solar cells Nat. Photon. 2012, 6, 153–161.
23. Turner , S. T.; Pingel, P.; Steyrleuthner , R.; Crossland , E. J. W.; Ludwigs , S.; Neher, D. Quantitative analysis of bulk heterojunction films using linear absorption spectroscopy and solar cell performance Adv. Funct. Mater. 2011 , 21 , 4640-4652
24. Szarko, J. M.; Rolczynski, B. S.; Lou, S. J.; Xu, T.; Strzalka, J.; Marks, T. J.; Yu, L.; Chen, L. X. Photovoltaic function and exciton/charge transfer dynamics in a highly efficient semiconducting copolymer Adv. Funct. Mater. 2014, 24, 10-26.
25. Young, T. J.; Monclus, M. A.; Burnett, T. L.; Broughton, W. R.; Ogin S. L.; Smith, P. A. The use of the PeakForce quantitative nanomechanical mapping AFM-based method for high-resolution Young's modulus measurement of polymers Meas. Sci. Technol. 2011, 22, 125703.
26. Dokukin M. E.; Sokolov, I. Quantitative mapping of the elastic modulus of soft materials with HarmoniX and PeakForce QNM AFM modes Langmuir 2012, 28, 16060-16071.
27. Schön, P.; Bagdi, K.; Molnár, K.; Markus, P.; Pukánszky B.; Vancso, G. J. Quantitative mapping of elastic moduli at the nanoscale in phase separated polyurethanes by AFM Eur. Polym. J. 2011, 47, 692-698.

28. Awartani, O.; Lemanski, B. I.; Ro, H. W.; Richter, L. J.; DeLongchamp, D. M.; O'Connor, B. T. Correlating stiffness, ductility, and morphology of polymer: fullerene films for solar cell applications Adv. Energy Mater. 2013, 3, 399-406.
29. Wang, D.; Liu, F.; Yagihashi, N.; Nakaya, M.; Ferdous, S.; Liang, X.; Muramatsu, A.; Nakajima, K.; Russell, T. P. New insights into morphology of high performance BHJ photovoltaics revealed by high resolution AFM Nano Lett. 2014, 14, 5727-5732.
30. Savagatrup, S.; Makaram, A. S.; Burke, D. J.; Lipomi, D. J. Mechanical properties of conjugated polymers and polymer-fullerene composites as a function of molecular structure Adv. Funct. Mater. 2014, 24, 1169-1181.
31. Savagatrup, S.; Printz, A. D.; Rodriquez, D.; Lipomi, D. J. Best of both worlds: conjugated polymers exhibiting good photovoltaic behavior and high tensile elasticity Macromolecules 2014, 47, 1981– 1992.
32. Gurau, M. C.; Delongchamp, D. M.; Vogel, B. M.; Lin, E. K.; Fischer, D. A.; Sambasivan, S.; Richter, L. J. Measuring molecular order in poly(3-alkylthiophene) thin films with polarizing spectroscopies Langmuir 2007, 23, 834-842.
33. Gather M. C.; Bradley, D. D. C. An improved optical method for determining the order parameter in thin oriented molecular films and demonstration of a highly axial dipole moment for the lowest energy π-π* optical transition in poly(9,9-dioctylfluorene-co-bithiophene) Adv. Funct. Mater. 2007, 17, 479-485.
34. O'Connor, B.; Kline, R. J.; Conrad, B. R.; Richter, L. J.; Gundlach, D.; Toney, M. F.; DeLongchamp, D. M. Anisotropic structure and charge transport in highly strain-aligned regioregular poly(3-hexylthiophene) Adv. Funct. Mater. 2011, 21, 3697-3705.

35. Cao, Y.; Smith, P.; Heeger, A. J. Mechanical and electrical properties of polyacetylene films oriented by tensile drawings Polymer 1991, 32, 1210-1218.

36. Pomfret, S.; Adams, P.; Comfort, N.; Monkman, A. Electrical and mechanical properties of polyaniline fibers produced by a one-step wet spinning process Polymer 2000, 41, 2265-2269.

37. Yasuda, T.; Han, L.; Tsutsui, T. Fabrication of stretch-oriented regioregular poly(3-hexylthiophene) film and its application to organic field-effect transistors J. Photopolym. Sci. Technol. 2009, 22, 713-717.

38. Lipomi, D. J.; Lee, J. A.; Vosgueritchian, M.; Tee, B. C. K.; Bolander, J. A.; Bao, Z. Electronic properties of transparent conductive films of PEDOT:PSS on stretchable substrates Chem. Mater. 2012, 24, 373-382.

39. Hagler, T.; Pakbaz, K.; Voss, K.; Heeger, A. Enhanced order and electronic delocalization in conjugated polymers oriented by gel processing in polyethylene Phys. Rev. B 1991, 44, 8652.

40. Dyreklev, P.; Berggren, M.; Inganäs, O.; Andersson, M. R.; Wennerström, O.; Hjertberg, T. Polarized electroluminescence from an oriented substituted polythiophene in a light emitting diode Adv. Mater. 1995, 7, 43-45.

41. Alvarez-Fernandez, A.; Maldonado, J.; Perez-Gutierrez, E.; Rodriguez, M.; Ramos-Ortiz, G.; Barbosa-Garcia, O.; Meneses-Nava, M.; Zolotukhin, M. G. Performance and stability of PTB7:PC71BM based polymer solar cells, with ECZ and/or PVK dopants, under the application of an external electric field J. Mater. Sci.: Mater. Electron. 2016, 27, 6271–6281.

## Chapter 5 Summary

Conjugated polymers exhibit superior properties to conventional semiconductor materials with regards to large-area thin-film form factors, mechanical compliance, solution processability, and low cost. These features play an important role in stretchable electronic devices, robotics and other applications. However, performance degradation over time or loading cycles needs to be addressed. Fundamental insights have been obtained to understand the failure in detail, which in turn helps to design and establish materials preferentially used in intrinsically stretchable devices. This research focuses on discovering the relationship between microstructure and mechanical stretchability on device performance. It is also an effort to enhance the performance of stretchable polymer light-emitting electrochemical cells (PLECs) and organic solar cells (OPVs).

The first part of work in this thesis developed a recipe of PLEC with an optimized luminescence, efficiency and stability on indium tin oxide (ITO) substrate, as a baseline of stretchable PLEC. A stable 6.0 cd/A efficiency PLEC device at 1500 cd/m$^2$ emission brightness on the ITO substrate is obtained. Here we used curable ionic conductive molecules to 1) provide the pathway for ions conduction to help form the p-i-n junction, and 2) the functional end groups in these curable ionic small molecules are polymerized during p-i-n junction formation to realize fast turn-on speed as well as stabilize PLEC performance. Meanwhile, in order to fulfill the purpose of stretchability, a soft medium poly(ethylene oxide) (PEO) with intermediate chain length was chosen as an additive to the ionic conductor. Phase morphologies were studied to understand the scale of phase separation impact on device

performance. The yellow fluorescent SY-PPV based PLECs with moderate amount of PEO and ETPTA exhibit fast response time, high electroluminescence and reasonable stability.

In light of the simple device structure, stretchable PLECs have been successfully made using a pair of silver nanowire-polyurethane (AgNW-PUA) substrates as electrodes. The PLEC device could be stretched up to 140% strain before luminescence decreased to 10%. The as formed interpenetrating polymer network (IPN) in the PLEC active layer exhibits rubbery elasticity at room temperature. The PLEC blend is composed of a porous phase, which helps to accommodate deformation along strain direction. Such deformation does not induce any orientation to SY-PPV polymer chains, and the polymer chains could retain their randomness at strains up to 100%. No anisotropic polarization properties can be seen from absorption or emission spectra. It highlights that the fabrication of intrinsically elastomeric polymer light emitting devices under large strain is expected to be possible by forming IPN morphology in the emissive layer.

Chapter 4 focuses on unveiling the morphological influence to enhance stretchability in an organic solar cell (OPV). This stretchable OPV can be elastically deformed up to 100%. With the aid of high boiling point additive 1,8-diiodooctane (DIO), not only the miscibility between PTB7 and $PC_{71}BM$ is improved by reducing $PC_{71}BM$ grain size, but also leaves free volume in the active layer. This free volume contributes to the elasticity in the OPV blend film where they can arrange the deformation by re-orientation of PTB7 within the grains and no net re-orientation to the entire PTB7 chains. This work highlights that free volume and smaller grains in the OPV blend would largely improve the elastomeric deformability in an otherwise brittle film.

The field of molecularly stretchable electronics is still in its infancy. The purpose of this research is to understand the molecular structural determinants of the mechanical properties to the semiconducting polymers, provide a methodology to characterize the nanoscale morphology with true Young's modulus, and develop a series of concept on how morphology feature from different molecular mixture system would impact the device stretchability. To this end, this study would also help to provide insights toward new materials synthesis that exhibit the best of both "worlds"—favorable mechanical and electronic properties.